FLOODRisk Master
Global Change • Hydroinformatics • Planning

Master Programme
in *Flood Risk Management*

Experimental study of threshold of sediment movement in high slope streams to analyse flood risk assessment in mountain rivers.

Chien-Chih Lin

MSc Thesis (1050898)
August 2019

Univerza v Ljubljani

UNESCO IHE DELFT
TECHNISCHE UNIVERSITÄT DRESDEN
UPC UNIVERSITAT POLITÈCNICA DE CATALUNYA BARCELONATECH

Experimental study of threshold of sediment movement in high slope streams to analyse flood risk assessment in mountain rivers.

Master of Science Thesis
by
Chien-Chih Lin

Supervisors
Prof. Allen Bateman Pinzon (UPC)

Examination committee

Prof. Allen Bateman Pinzon (UPC)
Prof. Vicente Cesar de Medina Iglesias (UPC)
Dr. Biswa Bhattacharya (IHE-Delft)

This research is done for the partial fulfilment of requirements for the Master of Science degree at the UNESCO-IHE Institute for Water Education, Delft, the Netherlands

Barcelona
August 2019

Acknowledge

It would not have been possible to write this M.Sc. thesis without the help and support of the kind people around me, to only some of whom it is possible to give particular mention here.

Above all, I would like to thank my supervisor Prof. Allen Bateman for his help and support. I have learned a lot from his advice and unsurpassed knowledge of the field of study. I would also like to thank Blanca Marin for her dedication during the six-month period. The thesis would not have been completed without her contribution to the collection of related experimental data.

I would like to acknowledge European Commission for the financial support and the four institutes UNESCO-IHE, Institute for Water Education, Delft, The Netherlands; Technical University of Dresden, Germany; Universitat Politecnica de Catalunya, Barcelona, Spain; and University of Ljubljana, Slovenia for their outstanding academic and technical support. I offer my sincerest gratitude to Dr. Biswa Bhattacharya, Prof. Dr. Allen Bateman, Prof. Dr. Dimitri Solomatine, Prof. Dr. Christian Bernhofer, and Prof. Dr. Mitja Brilly for their help and support throughout the study period.

I would like to convey my deepest gratitude to my parents, without their inspiration and sacrifice it was not possible for me to reach at this level of study and research.

Abstract

When it comes to the floods in high mountain rivers, it is vital to realize the initiation of sediment movement and sediment motion. In reality, these mechanisms will affect channel configuration, flow depth, and further flooding that occurs in high mountain rivers. Thus, the flood risk assessment needs to be reconsidered addressing such issue.

Shields (1936) proposed a comprehensive concept, as known as Shields diagram, to characterize the threshold condition of incipient motion. Nonetheless, scatter data in Shields diagram implied the subjectivity in determining the threshold of motion. Also, it did not take the slope effect into consideration.

The thesis aims to investigate the slope effect on the threshold of motion as well as the value of dimensionless shear stress, both conceptually and experimental. For theoretical method, the equilibrium of force acting on a sediment grain lying on a non-horizontal surface has been analysed. Furthermore, the threshold of movement and corresponding dimensionless shear stress have been derived from such relationship.

To confirm the method, experimental investigation has been conducted in a hydraulic channel situated in the Morphodynamics Laboratory of Department of Hydraulic, Maritime and Environmental Engineering of Universitat Politècnica de Catalunya. The experimental was conducted by altering the inclination angle and flow rate means to observe the visualization of threshold of motion. The size of the sediment grains is 14.5mm, assuming non-cohesive and uniform.

The experimental results indicate the dimensionless shear stress no longer remains constant when Reynold number is higher than $1.5x10^3$, and subsequently increases proportionally with increasing inclination angle, corresponding to Reynold number from $1.7x10^3$ to $1.9x10^3$. Such conclusion is contrast to the Shields diagram, which claimed the value of dimensionless shear stress remain 0.056 with respect to Reynold number higher than 10^3. Whereas, the thesis is subject to a few limitations. First of all, all of experimental investigation is at the condition of supercritical condition instead of critical condition assumed, owing to the limit condition of facilities. Secondly, the visualization method to recognize the experimental threshold of motion might result in the deviation of initiation for sediment entrainment.

In sum, thesis provides some hints to determine the threshold of motion regarding flooding in high mountain rivers. Nonetheless, to address the flood risk assessment, several issues still need to be examined carefully. Firstly, the study of the manning coefficient is required since it does not remain constant with regards to variation to slope angle. Secondly, how the channel configuration, flow depth, and floods are quantitatively affected need more investigation.

Table of Contents

List of figures

List of Tables

List of symbols

A	Cross-section area (m^2)
B	Buoyant force (N)
b	Measured length of weir crest (m)
b_e	Effective breadth (m)
C_D	Coefficient of drag force
C_e	Effective coefficient of discharge
C_f	Friction coefficient
C_L	Coefficient of lift force
d	Flow depth (m)
D	Median diameter of the sediment (m)
D_{50}/h	Relative roughness
F_D	Drag force (N)
F_L	Lift force (N)
Fr	Froude number
h^+	Velocity Normalized flow depth (m)
h_1	Head measured above the weir crest (m)
h_e	Effective head (m)
g	Gravitational acceleration (m/s^2)
J	Calibration coefficient
K	Von Karman constant
k_b	Effective breadth Coefficient
k_h	Effective head Coefficient
K_s	Relative roughness height(m)
n	Manning coefficient
N	Normal force (N)
Q	Discharge/ Flow rate (m^3/s)
Re^*	Particle Reynold number
Re^{*+}	Normalized Reynold number
R_h	Hydraulic depth (m)

S_f Energy slope

Ss Specific gravity

u^* Shear velocity (m/s)

U Mean velocity (m/s)

V_p Volume of the particle (m^3)

W_s Gravity force (N)

z height above bed (m)

τ_0 Bed shear stress (N/m^2)

τ_c Critical bed shear stress (N/m^2)

τ^* Dimensionless shear stress

τ^{*+} Normalized dimensionless shear stress

γ_s Specific weight of the sediment (N/m^3)

γ Specific weight of the fluid (N/m^3)

ν Kinematic viscosity of the fluid (m^2/s)

ρ Density of fluid (kg/m^3)

α Inclination angle

φ Angle of repose

Chapter 1. Introduction

1.1 Statement of the problem

Sediment transport is a significant component of flooding in the mountain rivers. For example, when the streamflow reaches to critical condition, the sediment motion initiates. Then, the following sediment transport is likely to alter the channel configuration, and the flow depth. In response to such issue, flood risk assessment needs to be reconsidered corresponding to such mechanisms. Thus, understanding the behaviours of threshold of sediment movement is essential. However, it is not well-understood due to the interaction of many parameters. Definition to the threshold condition for initial sediment movement is identified as prerequisite for the estimation of sediment transport. On account of unpredictable hydrodynamics as well as sediment dynamics, it is challenging to characterize sediment entrainment when flooding occurs. In response to such challenge, numerous empirical threshold curves have been proposed as a result of the threshold condition of sediment entrainment.

In 1936, Shields proposed the well-known Shields diagram. This led to the Shields parameter, indicating a ratio of bed shear stress to the submerged weight force of the grains. As a result of his contribution, the following studies have been developed, addressing the issue concerning threshold condition for incipient motion. Despite his notable contribution, there are inherent difficulties in the definition to the threshold of sediment entrainment. For example, the scatter data in Shields diagram still remained unsolved. Moreover, the slope effect on sediment particles has a significant impact on the threshold condition of sediment movement.

Over the past few decades, research following his work have contributed to refinement. For example, Chiew and Parker (1994) evaluated the threshold of condition for cohesionless particle grain lying on a non-horizontal slope. Dey (2003) investigated the threshold of sediment motion with a combination of transverse (across the flow direction) and longitudinal (streamwise direction) sloping bed.

Despite of numerous studies being carried out on this subject, the threshold of movement corresponding to slope effect still needs to be examined. In response, for the thesis a new conceptual method was proposed to investigate slope effect on the threshold condition of incipient motion. In order to examine the theoretical method above, the related hydraulic experiments were conducted to obtain the experimental results. More detail is included in the following section.

1.2 Statement of Purpose

1.2.1 Objective

The main objective of thesis is to shed light on the condition of threshold condition of sediment movement, assessing the effect of slope on sediment entrainment. This has been achieved by means of proposition of a conceptual method to analyse incipient motion on non-horizontal slope, and experimental data collection. The study has been carried out with the intention to meet the following specific objectives:

- Establish an analytical formulation of resultant forces acting on a particle considering the inclination angle.
- Carry out an experiment and gather the flume data to verify the formulation.
- Compare flume data to data in Shields diagram and discuss the discrepancy
- Attempt to determine the condition of threshold of movement at non-horizontal situation.
- Associated threshold condition of sediment movement with flood risk assessment.

1.2.2 Research questions

In response to the objectives mentioned above, numerous research questions have been presented:

- How does the slope effect influence on the dimensionless shear stress? And what is the difference between the non-horizontal and horizontal situation?
- What is the assumption regarding the application of theoretical method?
- Does the flume data collect in the experiment relate to the trend in Shields diagram? If not, can we explain it?
- Regarding the flume data collected, is new theoretical method appropriate for describing the slope effect on dimensionless shear stress?
- How did the research address the flood risk issue in high mountain area?

1.3 Scope and framework of the thesis

1.3.1 Scope of the thesis

The thesis focuses on an understanding of threshold condition for initial sediment entrainment on non-horizontal surface. The investigation of slope effect on critical condition for sediment entrainment has been investigated analytically and experimentally.

Initially, the related concept regarding threshold of movement as well as dimensionless shear stress was first proposed by Shields (1936). He developed the Shields diagram to

characterize the critical condition when sediment begans to move. Thus, the concept of dimensionless shear stress, as known as Shields parameter was established to quantify the bed shear stress as well as diameter of sediments. For the thesis, we applied the equilibrium of force analysis, obtaining the identical form as Shields parameter. However, such parameter is not appropriate at the condition of non-horizontal surface due to the difference made by resultant forces. To be more specific, the direction exerted by component of gravity force as well as buoyant force is different from how it did horizontally.

For conceptual analysis, in response to the pitfalls of Shields parameter, a modified concept regarding the dimensionless shear stress as well as threshold of movement was developed by analysing how the hydraulic forces and gravity force behaved corresponding to non-horizontal surface. By doing so, we could re-examine the Shields diagram with regards to influence made by slope.

For experimental analysis, it has been carried out in a 9m*0.6m*0.4m open hydraulic channel at the Morphodynamics Laboratory, Universitat Politècnica de Catalunya. Although some of condition is unlikely to be achieved, a few assumptions were made. Firstly, the experimental sediment grains were considered non-cohesive. In terms of the characteristic of sediment grains, the size of diameter ranges from 13-16mm, and the median diameter was regarded as 14.5mm, whose size belonged to crushed gravel. Secondly, regarding the flow condition, it was assumed to be uniform, meaning the flow depth remained constant in every section of the channel. Such experimental investigation allowed to examine the theoretical method and address the slope effect on the dimensionless shear stress and the threshold of motion.

Finally, we aim to address the influence of threshold of motion to the floods in high mountain rivers. To be more specific, the fluvial dynamic derived from the threshold of motion will be addressed. In addition, it is able to be related to the flood risk assessment with regards to flooding in high mountain rivers occurred.

In sum, the main objective of the thesis is to analysis the slope effect on threshold of sediment movement. The understanding of related concept might be applied to the floods occurred in high mountain rivers. Furthermore, it is able to be related to the flood issue as well as flood risk assessment.

1.3.2 Framework of the thesis

The thesis consists of six chapters. A brief overview of each chapter is presented in the following paragraphs.

In the first chapter *'Introduction'*, a general introduction is provided, which consists of three main parts, which are the statement of the problem, a brief description of purpose and the scope of the study.

The second chapter *'Literature Review'* is a review of the available literatures, explaining the physical background and the theories used to describe threshold condition of incipient motion. Following is the development of formulating the slope effect on the threshold of movement, which is also the main topic of the thesis.

The third chapter *'Materials and methodology'* introduces a new conceptual method to evaluate initiation of sediment entrainment at non-horizontal situation.

The fourth chapter *'Experimental set up'* introduces the experimental device that supports the experiments, as well as the related preparation and the experimental procedure.

The fifth chapter *'Results'* presents the flume data obtained from the experiment.

The sixth chapter *'Discussion'* aims to further analyse the experimental results and interpret its significance.

The seventh chapter *'Conclusion'* includes a summary of the conclusions obtained from each part that comprise the thesis. It also includes some lines of research acquired from the research results.

Chapter 2. Literature review

2.1 Introduction

The initiation of sediment motion is part of the fundamental issues in the field of sediment transport. Thus, the ability to quantify is very important in the field of hydraulic engineering. As far as physical definition of threshold of sediment movement is concerned, due to the increasing flow velocity, the subsequently increasing hydrodynamics forces acting on sediments will reach to a critical value. When the sediment particles are no longer to resist, the initial movement occurs. The stage that induces initial sediment movement is often called threshold of movement. The concept of threshold of movement plays a vital role in a serious of discipline, such as fluvial geomorphology, oceanographic, sedimentologic…etc. It also relates to the management of river systems and constitutes the fundamental mechanism of the sediment transport theory.

In this chapter, the very initial definition of threshold of sediment entrainment prior to Shields diagram will be examined, which consists of four initial common methods. Secondly, the origin of dimensionless shear stress derived from Shields diagram will be mentioned, including supplemental data incorporated into the original empirical curve. Thirdly, the limitation resulted from Shields diagram and consequent Shields parameter will reviewed. In response to such challenge, numerous studies were carried out for refinement. Last but not least, the way of force analysis addressing threshold of movement will be illustrated which related to the method associated with the thesis topic.

2.2 Definition of threshold of sediment movement

Empirical threshold curves have been developed in a variety of ways. Hjulström (1935) & (1939) published the famous Hjulström diagram, relating the mean flow velocity to the particle diameter for erosion, transportation and sedimentation. Sundborg (1956) explored modifications to the Hjulström diagram, representing threshold condition relating critical shear velocity to particle diameter. In addition, the cohesive part of the diagram was supplemented. Despite their simplicity, shortcoming have been found and there is space for improvement.

Buffington and Montgomery (1997) sorted out there are four common methods corresponding to definition of incipient motion, which are (1) extrapolation of bed load transport rates to either a zero or low reference value (e.g., Shields, 1936; Day, 1980;

Parker and Klingeman,1982); (2) visual observation (e.g.,Gilbert,1914; Kramer,1935; Yalin and Karahan,1979); (3) development of competence functions that relate shear stress to the largest mobile grain size, from which one can establish the critical shear stress for a given size of interest (e.g., Andrews, 1983; Carling, 1983; Komar,1987a); and (4) theoretical calculation (e.g., White, 1940;Wiberg and Smith, 1987; Jiang and Haft, 1993).

The first method is based on critical shear stresses associated with either a zero or low reference transport rate extrapolated from paired shear stress and bed load transport measurements. Values determined from this approach are sensitive to the extrapolation method (cf. Parker and Klingeman, 1982; Diplas, 1987; Ashworth and Ferguson, 1989; Ashworth et al., 1992) and the particular reference transport value that is chosen (Wilcock, 1988).

The second method, visual observation, depends on the definition of how much movement constitutes initial motion (e.g., Gilbert, 1914; Kramer, 1935; Neill and Yalin, 1969; Wilcock, 1988). Standardized definitions of incipient motion have been proposed on the basis of the number of grains in motion, the area of bed observed, and the duration of observation (Neill and Yalin, 1969; Wilcock, 1988). Visual observation is direct but subjective depending on one's definition of how much consists of incipient motion. Thus, it has not been widely accepted.

Competence functions used in the third method are sensitive to the size and efficiency of the sediment trap, sample size, sampling strategies, availability of coarse grain sizes and the curve-fitting technique (Wilcock, 1992b; Wathen et al., 1995). Furthermore, the competence method is inappropriate for sediment that exhibits equal mobility, as the competence approach relies on selective transport (Wilcock,1988, 1992b).

The fourth method utilizing simple force balance arguments to predict threshold of sediment movement is sensitive to model parameters such as grain protrusion, packing, and friction angle.

2.3 Shields diagram

Due to the difficulties defining the threshold conditions, numerous empirical threshold curves have been developed, including Shields diagram. Shields (1936) proposed the well-known Shields diagram, which is the most widely criterion for the threshold of sediment entrainment. A various of supplemental data (Gilbert, 1914; Kramer, 1935; Casey, 1935; USWES, 1935) were incorporated into Shields' experimental results, and thus the empirical threshold curve was established. Above this curve, the sediments are going to be set in motion, while below it the entrainment threshold is insufficient to

initiate sediment movement. The points for a bed load of uniform grain size and angular shape were plotted in the Shields curve, relating the dimensionless shear stress to the particle Reynolds number.

The dimensionless shear stress, known as Shields parameter, refers to $\tau^* = \frac{\tau_o}{(\gamma_s - \gamma)D}$, where τ_o is bed shear stress; γ_s is specific weight of the sediment; γ is specific weight of fluid; D is median diameter of the sediment particle; g is gravitational acceleration. The particle Reynolds number refers to $\mathrm{Re}^* = \frac{u^* D}{\nu}$, where u^* is the critical shear velocity; ν is the kinematic viscosity of the fluid. The critical shear stress is reached when the movement of a particle occurs thus $\tau_o = \tau_c$.

In Shields diagram, four regions were distinguished in terms of the thickness of the layer. In the first region the thickness of the laminar layer is greater than the mean grain size, and the trend is considered straight smooth line, obtained by extrapolation. For the value of the dimensionless critical shear stress, it is found that $\tau^* = \frac{0.1}{Re^*}$, when $\mathrm{Re}^* < 2$. In the second region, the thickness of the laminar layer is of the same order of the magnitude as the mean grain size. Shields considered value of $\tau^* = 0.03$, for $\mathrm{Re}^* = 10$. As far as the third region is concerned, the layer thickness becomes small that flow resistance is exclusively governed by eddy formation. The flow is subject to the quadratic resistance while that resistance of the grain is far from significant. The roughness decreased with increasing Reynold number. Thus, the dimensionless shear stress is increasing until $\mathrm{Re}^* = 10^3$. For the fourth region not only the quadratic resistance but also resistance of grain involved. When $\mathrm{Re}^* > 10^3$, for gravels and coarser, Shields suggested a constant value of dimensionless shear stress $\tau^* = 0.06$, whereas appropriate value for this constant has been widely discussed.
Still, some concerns have been mentioned by Shields (1936). Firstly, the constant value might be overestimated by extrapolation as a result of the sediment grains as well as the bed features. Additionally, the flow conditions derived from USWES (1935) were not uniform whereas the rest of the data set are uniform.

2.4 Limitation to Shields diagram

Despite the success of Shields' work, great quantities of researchers (Miller et al., 1977; Yalin and Karahan, 1979; Buffington and Montgomery, 1997; Buffington, 1999) expressed the concerns to the Shields diagram.

First of all, Buffington (1999) identified some of the inconsistencies in the related literature to Shields' work, which is due to limited access to the original work. Incomplete or inaccurate description regarding Shields' work comes from second-hand descriptions

in textbooks and journal articles. The scientific literature is rife with misconceptions and errors regarding Shields' methods and results.

Secondly, the interpretation to determine threshold condition of incipient motion is well-debated. The experimental data scatter in original empirical curve revealed that sediment entrainment is a random process (Paphitis 2001). Due to the complex functions controlling the threshold condition, thus deterministic definitions of the threshold condition are limited (Neill and Yalin, 1969; Buffington and Montgomery, 1997).

Furthermore, the experimental sediments employed in empirical curve were not uniform in size but rather mixtures (Buffington and Montgomery, 1997; Buffington, 1999). On one hand, Shields referred to the work of Kramer (1932, 1935), Casey (1935), and USWES (1935), as being representative of mixed-size sediments. On the other hand, he also claimed that his curve with these supplemental data was representative of uniform-size sediments. However, mixture median sediment sizes will be equivalent to surface median sediment sizes only when laboratory sediment mixtures are well sorted. Different dimensionless shear stress scaled by either the mean or median size of the sediment mixture may result in some of the scatter of Shields' results.

Another explanation to amount of scatter in Shields curve might have stemmed from the mixed reference-based and visual-based incipient-motion approaches. Initially Shields probably defined incipient-motion thresholds by extrapolating stress-transport relations to zero transport rate, as is popularly believed. In contrast, he defined incipient motion values for supplemental data sources using two differing thresholds of visually based movement. Both methods might result in different values of dimensionless critical shear stress, whereas Shields failed to clearly indicate which method was employed. Shields did not correct the form drag caused by the presence of bed forms, and thus values of dimensionless critical shear stress differs. Although Shields applied a sidewall correction, he did not attempt to correct calculated basal shear stresses for bed-form drag. As with Shields' work, form drag was not accounted for in these supplemental data (Gilbert, 1914; Kramer, 1935; Casey, 1935; USWES, 1935).

Subsequently, modifications of the Shields curve have been proposed. Miller et al. (1977) reviewed the threshold of movement under unidirectional flow to examine the empirical curves by means of additional sets of available data. The data were exclusively obtained from open channel flumes with parallel sidewalls where flows were uniform and steady over flattened beds of uniform granular, rounded sediments. Such condition was introduced to remove unmanageable amount of scatter in the data. Nevertheless, the revised version of empirical threshold relationships is limited to certain combinations of grain density, fluid density, fluid viscosity and gravity. The empirical curves and relationships are required to be properly employed under severe restrictions.

Paphitis (2001) investigated existing experimental data set on sediment threshold under unidirectional flow conditions. Simple analytical formulae are derived describing single line curves for mean threshold values and envelopes for the initial movement of discrete particles and the commencement of mass sediment transport phases of the critical condition. He revealed the limitation of deterministic solutions due to the complexity of factors governing the prevailing threshold conditions. The definitive threshold condition under certain grain size is not able to be displaced, but rather that a range of threshold values exist. Since the critical condition has been interpreted in various ways, the formulae have to be treated with caution in applications.

2.5 Influence of slope effect on the threshold of movement

One of the earliest experimental results addressing the slope effect was conducted by Luque and van Beek (1976), suggesting that the critical shear stress required for the initial movement of sediment on a sloping bed decreases with increase in slope. Whitehouse and Hardisty (1988) conducted experiments on both adverse and streamwise bed slopes to examine the effect of bed slopes and angle-of-repose on sediment threshold.

Chiew and Parker (1994) investigated the effect of streamwise bed slopes on the initiation of sediment entrainment, confirming that the streamwise bed slope has an important influence on the threshold condition for sediment entrainment.

One of the issues is that when the slope is steep or adverse, it is unlikely to maintain the uniform flow. Instead of conducting experiments in open channel flow, their test conducted with closed-conduit flow thus avoid the problem associated with uniform flow. Considering the resultant forces (lift force, drag force, buoyant force and gravity force) acting on a cohesionless particle lying on a bed consisting of similar particles, the slope effect on initial sediment transport can be addressed. The forces acting tangential (Ft) and normal to the bed (Fn) are related to the angle of repose of the sediment (φ), where $\tan\varphi = Ft / Fn$. The ratio of the critical shear stress at any streamwise bed slope (α) to the corresponding value at $\alpha = 0$ is written as:

$$\frac{\tau_c}{\tau_0} = \cos\alpha\left(1 - \frac{\tan\alpha}{\tan\varphi}\right) \tag{2-1}$$

where τ_c is critical shear stress; τ_0 is critical shear stress for horizontal slope.

In terms of shear velocity, the relationship takes the form

$$\frac{u_c^*}{u_0^*} = \sqrt{\cos\alpha\left(1 - \frac{\tan\alpha}{\tan\varphi}\right)} \tag{2-2}$$

When u_c^*/u_0^* is plotted as a function of θ/φ, it is found the effect of the streamwise bed slope on the threshold condition for sediment entrainment adequately describes the incipient condition for the transport of sediments lying on streamwise slopes ranging from steep downward to zero.

The equation above derived from force analysis was used to determine the critical shear stress for sediment lying on a non-horizontal slope. Many investigators (Stevens et al. 1976; Luque and van Beek. 1976; Howard. 1977; Allen. 1982; Whitehouse and Hardisty. 1988; Iversen and Rasmussen. 1994; Dey et al. 1999; Dey and Debnath. 2000) used the similar form of equation.

Nevertheless, Christensen (1994) pointed out the that the force analysis mentioned by Chiew and Parker (1994) has its pitfalls. The buoyant force acting on the individual particle is not vertical when the water surface is sloping. It is supposed to be perpendicular to the water surface and not able to be combined with the particle weight. Thus, at the condition of uniform flow, the formula for slope correction is supposed to be rewritten as:

$$\frac{\tau_c}{\tau_0} = \cos\alpha \ \left(1 - \left(\frac{\rho_s}{\rho_s - \rho}\right)\frac{\tan\alpha}{\tan\varphi}\right) \tag{2-3}$$

Apart from that, Dey (2003) presented an investigation on the threshold of non-cohesive sediment movement under a steady-uniform stream flow combing both transverse (across the flow direction) with longitudinal (streamwise direction) sloping bed in theoretical and experimental way. The experiments were carried out in closed-conduit flow for three sizes of uniform sediments by applying to the side-wall correction, with an eye to determining shear stress. Theoretical analysis of the equilibrium of a sediment particle lying on a combined transverse and longitudinal sloping bed implies that the critical shear stress ratio (ratio of critical shear stress for a sloping bed to that for a horizontal bed) is a function of the transverse bed slope, longitudinal bed slope, angle of repose of sediment particles, and lift-drag ratio.

In addition to theories mentioned above, another theoretical analysis addressing the equilibrium of forces of a gravel particle in a high sloping streamwise is based on the relative degree of exposure of the particle itself to the streamflow. It is suggested that when the slope is increasing, the influence of exposure of a particle on the hydrodynamic forces reinforces, which results from the increasing velocity with regards to the degree of exposure. (Armanini and Gregoretti 2005).

Gregoretti (2008) further established relationships between mean streamflow depth and cohesionless particle bed characteristics at the commencement of the sediment entrainment with respect to high slopes, at the condition of low submergence. Using a

low-submergence flow velocity profile in the particle balance of forces at the limit of equilibrium leads to a relationship between the mean flow depth and the sediment size. Another velocity profile of low-submergence flow is introduced to that used in the previous study, and two analytical expressions of flow depths corresponding to the beginning of sediment transport are obtained for both fully submerged particles and partially submerged particles. The theoretical flow depths given by the analytical expressions are then compared with those from previous experimental tests at the beginning of sediment transport at high slopes with fully submerged particles. The comparison indicates a satisfactory agreement between theoretical and experimental values of flow depth corresponding to the degree of exposure and the relative position of the exposed part of the surface layer bed particles.

Nonetheless, Recking (2009) and Lamb et al. (2008) claimed that given the amount of flume and fields data, critical dimensionless shear stress for incipient motion in open-channel flow increases with channel slope, indicating particles of the same size are more stable on steeper slopes, whereas contrary to the usual assumption that owing to the downstream gravitational force, critical Shields stress decreases at steep slopes.

In order to confirm the assertion, Recking (2009) utilized the flume and fields experimental measurements to reproduce a force balance model, provided a more compatible velocity profile with available velocity measurements over gravel beds was implemented, replacing the classical logarithmic velocity profile. For his research, the flow resistance data was utilized to fit a velocity profile including a roughness layer, on the basis of depth average velocity measurements. Such data was used in a force balance model for incipient motion, which adequately reproduced the critical Shields stress increase with increasing slope. Yet, several aspects deserve further investigation. For example, the roughness layer properties, the drag and lift coefficient variation with relative depth as well as slope, and the effects of slope on the hiding function for field applications with non-uniform sediments.

Lamb et al. (2008) proposed a model for the local velocity within the grain-roughness layer based on a 1-D eddy viscosity with wake mixing. In addition, the magnitude of near-bed turbulent fluctuations is shown to depend on the depth-averaged flow velocity and the relative roughness. Extension of the model to mixed grain sizes indicates that the coarser fraction becomes increasingly difficult to transport on steeper slopes.

2.6 Summary

The limitations to Shields curve have been pointed out by many researchers. When it comes to the experimental scatter data in the empirical curve, it may have attributed to amount of subjectivity and judgment to determine the threshold of movement.

Furthermore, entrainment of sediment particles is a random process. The randomness of this process inevitably led to somewhat differing definitions of the threshold condition by various researchers (Paphitis 2001).

As far as slope effect on threshold of sediment entrainment is concerned, Chiew and Parker (1994) conducted an experimental analysis, revealing that the streamwise bed slope has an important influence on the threshold condition for sediment entrainment. Nevertheless, at a non-horizontal surface, the buoyant force has been integrated into the submerged weight force. Nevertheless, Christensen (1994) proposed the buoyant force acting on the individual particle is not perpendicular to horizontal surface but perpendicular to water surface. Thus, such inappropriate equilibrium of force requires further research. Thus, the correction is main focus in the thesis, and it is going to be presented in the next chapter.

Chapter 3. Materials and Methodology

3.1 Introduction

In response to the need for the assessment of threshold condition of sediment entrainment concerning slope effect, this chapter illustrates a conceptual method related to slope issue to dimensionless shear stress by studying the resultant forces acting on an individual sediment grain.

Section 3.2.1 initiates the origin form of Shields parameter by means of the analysis of resultant forces acting on a sediment particle on horizontal surface. Section 3.2.3 further examines the slope effect on dimensionless shear stress by means of force analysis. Section 3.2.4 discusses the influence of bed geometry on bed shear stress.

3.2 Description of Shields diagram

Threshold of sediment movement, as known as incipient motion, is the critical condition at which sediment particles start to move. Shields (1936) established the threshold condition, concluding that the dimensionless shear stress (τ^*), as known as Shields parameter, is a function of bed shear stress (τ_0), as well as the median diameter of sediment particle (D). Eq. 3-1 depicts dimensionless shear stress is composed of bed shear stress as well as median diameter, where γ_s is specific weight of particle; γ is specific weight of fluid. Eq. 3-2 describes bed shear stress, being as a function of hydraulic radius (R_h) as well as energy slope (S_f).

$$\tau^* = \frac{\tau_0}{(\gamma_S - \gamma)D} \tag{3-1}$$

$$\tau_0 = \gamma\, R_h\, S_f \tag{3-2}$$

$$Re^* = \frac{u^*\, D}{v} \tag{3-3}$$

Based on both equations above, it can be assumed that the when a particle initiate its motion, the bed shear stress also becomes critical, and thus bed shear stress can be recorded as $\tau_0 = \tau_{cr}$.

In addition, at the threshold condition, for gravels and coarser, the value of dimensionless shear stress is considered a constant value 0.056 corresponding to the particle Reynold number (Re^*) higher than 10^3. The Reynold number is depicted in Eq. 3-3, where u^* is

shear velocity; v is kinematic viscosity of the fluid. Below is the Shields diagram regarding dimensionless shear stress and Reynold number (Figure 3-1).

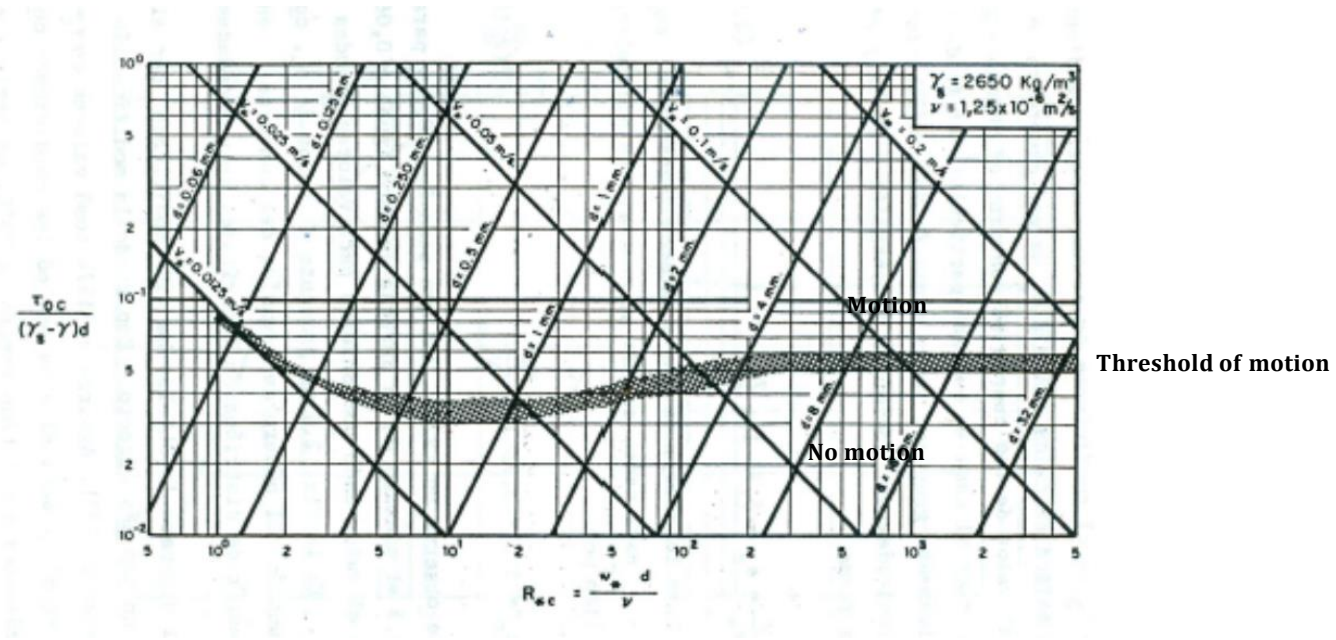

Figure 3-1 Shields diagram

3.3 The derivation of the dimensionless shear stress

3.3.1 Analyse the dimensionless shear stress by means of force analysis (horizontal surface)

Prior to discussion when it comes to the non-horizontal situation, it is reasonable to characterize dimensionless shear stress by approaching the forces acting on a sediment particle.

As mentioned in Eq. 3-1, the Shields parameter is basically composed of bed shear stress and median sediment grain. Likewise, such form can be obtained by means of equilibrium of force.

The initial concept of the Shields parameter can be regarded as the ratio of the destabilizing force (applied hydraulic force) and the stabilizing force (resisting force by a sediment grain located at the bottom of a stream). Eq. 3-4 indicates the relationship of such ratio, which consists of Shields parameter.

$$\tau^* = \frac{\tau_0 * A \quad \text{(destabilizing force)}}{W_s - B \quad \text{(stabilizing force)}} \tag{3-4}$$

Where F_D represents drag force ($\tau_0 * A$), being destabilizing force; A is cross-section area of sediment grain; W_s is gravity force; B is buoyant force. Figure 3-2 states how resultant forces act on a sediment particle at the condition of horizontal surface.

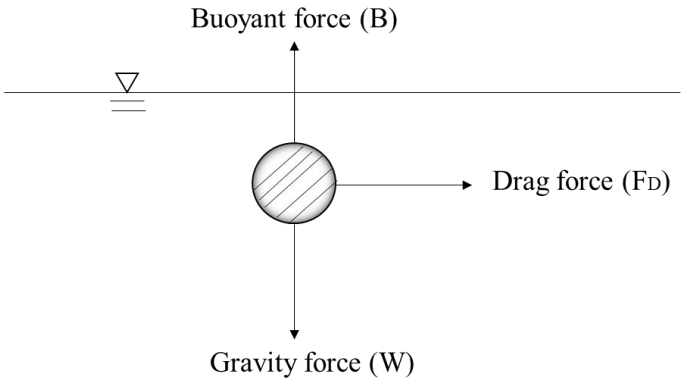

Figure 3-2 Resultant forces acting on a grain (horizontal surface)

In order to further quantify the relationship between dimensionless shear stress and bed shear stress, each force in Eq. 3-4 could be divided by the cross-section area (A). Thus, Eq. 3-4 can be written as:

$$\tau^* = \frac{\tau_0}{(\frac{\gamma_s V_p - \gamma V_p}{A})} \tag{3-5}$$

where submerged weight force, $W = \gamma_s V_p$; buoyant force, $B = \gamma V_p$; V_p is volume of particle.

Since dividing V_p by A becomes ($\frac{2}{3}D$), appropriate substitution of Eq. 3-5 yields

$$\tau^* = \frac{\tau_0}{\frac{2}{3}(\gamma_S - \gamma)D} \tag{3-6}$$

Such formula (Eq. 3-6) derived from force analysis corresponds to Shields parameters proposed in the Shields diagram; whereas the constant ($\frac{2}{3}$) arises from the relationship between volume and diameter of the particle.

3.3.2 Dimensionless shear stress by means of force analysis (non-horizontal surface)

As mentioned in Eq. 3-4, the dimensionless shear stress is the ratio of the destabilizing force to the stabilizing force. In response, Eq. 3-7 presents a new method to describe

dimensionless shear stress under the condition of inclination angle (α). The destabilizing forces are drag force (F_D) as well as the component of gravity force ($w_s \sin\alpha$), whereas stabilizing forces are the component of gravity force ($w_s \cos\alpha$), buoyant force (B), and life force (F_L). Thus, the assumed Shields parameter considering the inclination angle (α) is presented below:

$$\tau^* = \frac{F_D + w_s \sin\alpha}{w_s \cos\alpha - B - F_L} \tag{3-7}$$

Among these forces, the drag force is expressed as Eq. 3-8, whereas the life force is presented as Eq. 3-9. Both are associated with the product of shear stress and cross-section area.

$$F_D = \frac{1}{2} C_D \tau_0 A \tag{3-8}$$

$$F_L = \frac{1}{2} C_L \tau_0 A \tag{3-9}$$

Where C_D is the coefficient of drag force; C_L is the coefficient of lift force. For the thesis, we assumed values both are 1.

Likewise, the gravity force as well as the buoyant force can be expressed as the form consists of grain volume (V_p) and specific weight of particle (γ_s), shown below in Eq. 3-10 and Eq. 3-11, respectively. In terms of the buoyant force, it is set up normal to water surface instead of horizontal surface. Thus, it is associated with the inclination angle (α).

$$W_S = \gamma_s V_p \tag{3-10}$$

$$\mathrm{B} = \gamma\, V_p \cos\alpha \tag{3-11}$$

When examining the conceptual dimensionless shear stress, it is obviously a bit different from the way Shields proposed, without considering the influence brought by slope. Comparing with the original Shields parameter, the new dimensionless shear stress derived from Eq. 3-7 is supposed to be higher. First of all, in terms of the destabilizing force acting as numerator, the new one is higher than initial one. Secondly, the new stabilizing force being denominator is equal or lower. In sum, such ratio is supposed to be higher, suggesting higher value of dimensionless shear stress as a result of slope. Such conceptual proposition is going to be examined by means of experimental investigation.

3.4 Equilibrium of force with regards to slope effect

In this section, a theoretical method is used to present the equilibrium of forces acting on a particle under the condition of inclination angle (α). Figure 3-3 depicts the resultant force acting on a particle lying on non-horizontal surface with respect to inclination angle (α).

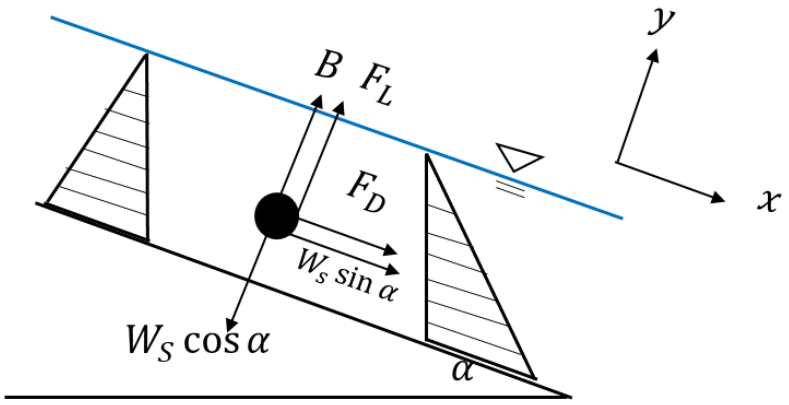

Figure 3-3 Conceptual resultant forces acting on a grain (non-horizontal surface)

Initially, in terms of x-direction, the equilibrium of the force can be written as:

$$\frac{1}{2}\tau_0 A + w_s \sin\alpha = \mu N \tag{3-12}$$

Whereas regarding y-direction, the normal force (N) acting on a particle is equal to:

$$\mathrm{N} = w_s \cos\alpha - B - \frac{1}{2}\tau_0 A \tag{3-13}$$

After combing both Eq. 3-10 and Eq. 3-11, a new formula can be written as:

$$\frac{1}{2}\tau_0 A + w_s \sin\alpha = \tan\varphi\,(w_s \cos\alpha - B - \frac{1}{2}\tau_0 A) \tag{3-14}$$

Where φ represents the angle of repose; When each term in Eq. 3-7 is divided by the cross-section area, it becomes:

$$\frac{1}{2}\tau_0 + \frac{w_s}{A}\sin\alpha = \tan\varphi\,(\frac{w_s}{A}\cos\alpha - \frac{B}{A} - \frac{1}{2}\tau_0) \tag{3-15}$$

Where the value of $\frac{w_s}{A}$ equals to $\frac{2}{3}\gamma_s \mathrm{D}$, and the value of $\frac{B}{A}$ is $\gamma \mathrm{D}\cos\theta$. Then after appropriate substitution, it yields:

$$\frac{1}{2}\tau_0 + \frac{2}{3}\gamma_s \mathrm{D}\sin\alpha = \tan\varphi\left(\frac{2}{3}\gamma_s \mathrm{D}\cos\alpha - \frac{2}{3}\gamma \mathrm{D}\cos\alpha\right) - \frac{1}{2}\tan\varphi\,\tau_0 \qquad (3\text{-}16)$$

In response to calibration, a coefficient (J) is put into practice. Then, such coefficient (J) is determined afterwards by means of experimental results. In sum, the equation becomes:

$$\tau_0 \frac{\left(\frac{1}{2}+\frac{1}{2}\tan\varphi\right)}{\frac{2}{3}\gamma D} = \mathrm{J} * ((\mathrm{Ss}-1)\cos\alpha\tan\varphi - Ss\sin\alpha) \qquad (3\text{-}17)$$

Where Ss is the specific gravity.

3.4.1 Limitations of the conceptual method

First of all, the conceptual method which addresses the forces acting on the particles does not consider forces that exerted by other particles. Although the hydrodynamic forces as well as submerged weight forces are considered in the conceptual method, the clamping forces between each particle have a significant impact on determining the threshold of motion.

In addition, for the thesis, the conceptual method considered the configuration of the cross-section area to be rectangular. Nonetheless, the setting might be inappropriate due to its simplification. Consequently, for the further investigation, to set up as triangle, trapezoid, or parabolic is more realistic.

3.5 Hydraulic variables

3.5.1 Froude number

In general, for rectangular cross-sections with uniform depth d, the Froude number (Fr) is defined as $\mathrm{u}/\sqrt{gd}$, where u is flow velocity. While considering the slope effect (α), the flow depth has to be corrected as ($\mathrm{d}\cos\alpha$). Thus, after correction, the Froude number is defined as:

$$\mathrm{Fr} = \mathrm{u}/\sqrt{gd\cos\theta} \tag{3-18}$$

For Fr < 1 the flow is called a subcritical flow; whereas for Fr > 1, the flow is characterised as supercritical flow. When Fr is equal to 1, the flow is denoted as critical flow.

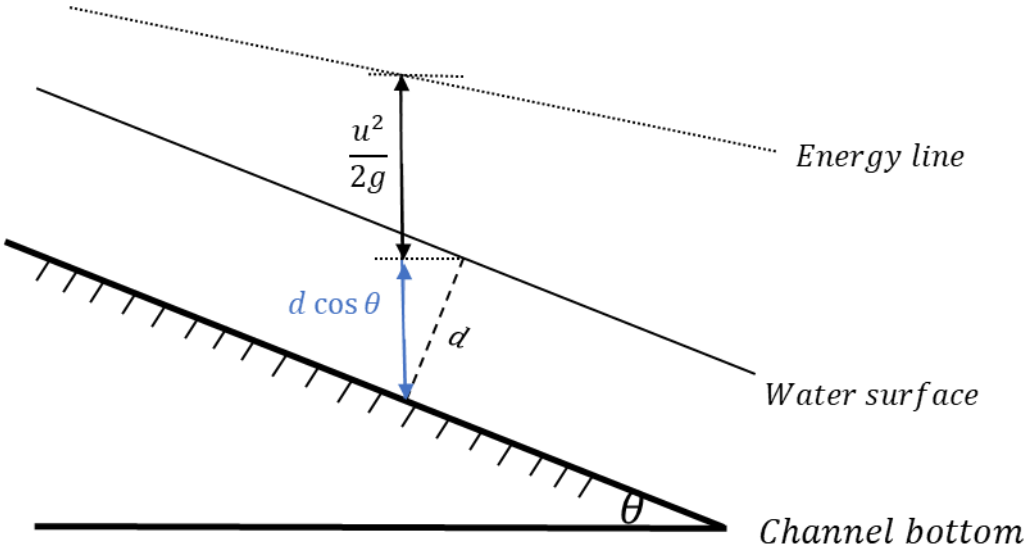

Figure 3-4 The head in open-channel flow

3.5.2 Friction coefficient

The flow resistance coefficient is used to evaluate the forces exerted by the boundaries and other factors associated with the flow that compensate for the gravity force by producing energy losses. Various characteristics affect the value of flow resistance coefficient, such as diameter of grain, and shape of grain.

The friction coefficient (C_f) is related to the roughness brought by the bed shear stress (τ_0). It is the ratio of the shear velocity (u^*) to mean flow velocity (U) (Eq. 3-19); whereas the shear velocity is expressed as Eq. 3-20.

$$C_f = \frac{u^{*2}}{U^2} \tag{3-19}$$

$$u^* = \sqrt{\frac{\tau_0}{\rho}} \tag{3-20}$$

3.5.3 Manning coefficient (n)

The Manning coefficient (n) is obtained from Manning equation (Eq. 3-21), which is an empirical formula to establish the relationship between the flow velocity, and thus flow discharge. Nonetheless, in reality, it is difficult to determine the value since a few factors that affect the value of Manning coefficient, such as vegetation, material involved, degree of irregularity, and variation of channel cross-section.

$$\mathrm{Q} = \frac{1}{\mathrm{n}} * \mathrm{A} * R_h^{\frac{2}{3}} * S_f^{\frac{1}{2}} \tag{3-21}$$

3.5.4 Relative roughness height (k_s)

Nikuradse (1933) studied the behavior of different sizes of sand in pipeline revetment and proposed the relative roughness height (k_s). The relative roughness height is related to effects of placement, packing density. Keulegean (1938) applied it for channels and further proposed the relationship between the local mean velocity (U) and the shear velocity (u^*) regarding turbulent flow (Eq. 3-22).

$$\frac{U}{u^*} = \frac{1}{K} \ln \left(\frac{11z}{k_s}\right) \tag{3-22}$$

Where K is the Von Karman constant (0.4); z is height above bed.

3.6 Summary

In this chapter, a conceptual method to investigate slope effect on threshold of sediment entrainment has been presented. Initially the analysis followed the general definition of threshold of motion, as proposed by Shields (1936), whereas the difference is that further investigation to address the slope effect was evaluated in the way of equilibrium of force.

It is noticeable that in most of previous studies, the buoyant force is considered upward force acting on a sediment grain submerged in the fluid, as a result of combination with weight force. For this thesis, when it comes to non-horizontal situation, the buoyant force acting on the sediment grains is not vertical with respect to horizontal surface but perpendicular to the water surface. The subtle difference caused by the direction of resultant force have a tremendous impact on the analysis of threshold of sediment movement.

In addition, according to new form of dimensionless shear stress (Eq. 3-7), the value of dimensionless shear stress proposed is supposed to be higher. When the inclination angle increased, the influence made by the component of gravity force is significant ($w_s \sin \alpha$), resulting in the increase in the destabilizing force, and thus greater ratio of dimensionless shear stress.

Chapter 4. Experimental set up

4.1 Introduction

In chapter three, a theoretical method addressing slope effect on the threshold of sediment movement has been proposed. As mentioned earlier, one of objectives is to conduct an experimental analysis to gather the related flume data, confirming the conceptual method.

In terms of the experimental analysis, the investigations related to the preparation as well as the set-up are introduced in this chapter. In section 4.2, the characteristics of laboratory facilities are introduced, such as the hydraulic flume for the experiment. In addition, the flow-rate measurement was conducted by means of rectangular weir, with an electromagnetic flowmeter as reference. More importantly, the calibration corresponding to such measurements are discussed. Section 4.3 describes the procedure to filter the sediment particles as well as the characteristic of the materials. Section 4.4 explains the experimental deign. Section 4.5 introduces the experimental procedure as well as the measurements during the experiment.

4.2 Laboratory facilities

The experiments were conducted in a hydraulic channel of the Morphodynamics Laboratory of Department of Hydraulic, Maritime and Environmental Engineering of Universitat Politècnica de Catalunya.

The hydraulic channel's dimensions are 9 m length, 0.4 m width, and 0.6 m depth rectangular channel. The side walls of the channel are made of glass, making it possible to observe and record flow characteristics as well as hydrodynamic data.

Two tanks are connected to each other by a pumping system, forming the recirculation system. The upstream tank discharges into the channel, receiving the water propelled by the pumps. The channel flushes the water into the downstream tank through the rectangular weir. At the downstream channel a grid plate is installed, and quantities of stones are placed, serving as an obstacle to prevent the experimental sediment particles from entering into the tank.

Channel slope was adjustable by means of traction pulley that tilted the flume about a pivot at its midpoint. The maximum slope angle can reach to 30^0.

The water-depth measurement is achieved using a level water gauge. The flow-rate measurement is operated by calculating the volume of rectangular weir situated in the downstream tank. Besides, it is calibrated by volumetric measurement. Simultaneously the electromagnetic flowmeter has access to valves, acting as a reference.

4.2.1 Water depth measurement

The method to measure the water depth is by a level water gauge, located near the downstream tank. The level water gauge is placed with an inclination angle of 30 degree. In other words, when 1mm increase is indicated by the level water gauge, water depth of the tank is increased to 0.5mm.

Figure 4-1 The measurement by means of water gauge

4.2.2 Calibration for water depth measurement

In order to correlate the zero point of the rectangular thin-plate weir to the zero point of the water gauge, performing a calibration is needed. A series of measurement has been made with a limnimeter which enables to relate the water level of the rectangular thin-plate weir to the measurement made by the water gauge. The principle of reset is that given the constant supply discharge, when the flow no longer exceeds from the weir, the water depth measurement initiates. A calibration curve has been made, connecting the increase of weir height to the increase in water depth suggested by the water gauge, given the discharge measured by electromagnetic flowmeters as a reference.

Table 4-1 presents a number of evaluations with respect to the measurement of water depth made by piezometer as well as limnimeter, the measurement made by electromagnetic flowmeters as reference.

Point	H piezometer (cm)	H limnimeter (cm)	Discharge (l/s)
0	0	102.82	0
A	5.6	105.81	3
B	17.9	111.5	16
C	19.8	112.29	19
D	20.3	112.77	20
E	18.4	111.95	17.5
F	13.6	109.06	10
G	8.8	107.2	6
H	3.9	104.86	2
I	2.6	104.15	1

Table 4-1 The comparison of water depth measurement

4.2.3 Flow-rate measurement (rectangular weir)

The flow-rate measurement has been executed, by calculating the discharge through a rectangular weir located in the downstream tank. Then, it was corroborated by volumetric measurement for calibration. In addition, each flow-rate measurement is referenced using the piezometer.

The calculation corresponding to rectangular weir is based on a method proposed by Kindsvater and Carter (1957). This method is mainly associated with the calibration rating of rectangular thin-plate weir, which can be applied to both fully and partially contracted rectangular weirs. For the present experiments, the weir located in the upstream tank is considered a partially contracted rectangular weir, owing to the proximity of the walls tank of the approach channel to the weir. The basic equation for the Kindsvater-Carter (1957) method is:

$$Q = \frac{2}{3} \cdot C_e \cdot (2g)^{1/2} \cdot b_e \cdot {h_e}^{\frac{3}{2}} \qquad (4\text{-}1)$$

Where:

Q is the discharge (m^3/s)

C_e is the effective coefficient of discharge (-)

g is the acceleration of gravity (m^2/s)

b_e is the effective breadth (m), equals to $b_e = b + k_b$. Where b is the measured length of weir crest (m)

h_e is the effective head (m), equals to $h_e = h_1 + k_h$. Where h_1 is the head measured above the weir crest (m)

The coefficient k_b and k_h represent the combined effects of the several phenomena due to viscosity and surface tension, respectively. The factor k_b changes with different ratios of crest length, b, to average width of approach channel, B. The values of k_b as a function of ratio b/B ranging from 0 to 1 are given on Figure 4-2. The factor k_h is a constant value equal to 0.001 m.

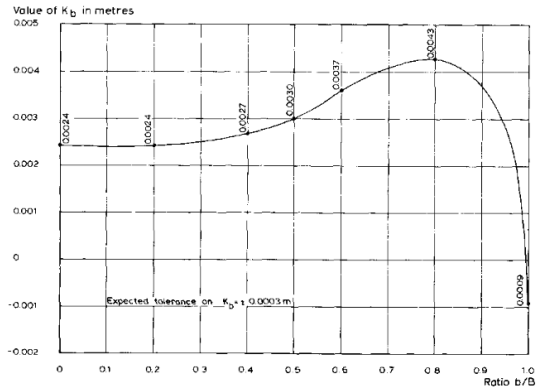

Figure 4-2 k_b as a function of b/B

Table 4-2 presents the water height of the tank, as well as the measurement taken by level water gauge, in order to calibrate the value of discharge with respect to volumetric measurement.

Discharge (l/s)	Water gauge (cm)	Weir height (cm)	Calculated discharge (l/s)
1	2.45	1.29	1.06
3	5.2	2.6	2.88
5	7.45	3.68	4.77
10	12.7	6.2	10.27
15	16.65	8.1	15.24
20	20.17	9.75	20.1

Table 4-2 The calculated flow rate by means of rectangular weir

4.2.4 Calibration for flow-rate measurement (volumetric measurement)

The calibration for flow-rate measurement has been implemented based on volumetric measurement performed in the upstream tank. In addition, since two magnetic flowmeters have connection to their corresponding valves, in charge of flow discharge, calibration taken by volumetric measurement is a guarantee of accuracy for magnetic flowmeters.

In principle, the measurement of volumetric measurement is divided into two parts: the investigation measuring the area of the upstream tank, and subsequently the height difference. The calculation of the area of the upstream tank has to be considered the area of water dump as a result of subtraction. Secondly, the height difference calculation is

that given the time, measuring the height difference of the upstream tank can further reach to its volume corresponding to its height difference.

The area of upstream tank

It is noticed that inside the upstream tank there is a water dump, serving as a resistance to overflow. Thus, the area of the dump act as a subtraction when calculating the area of the tank. The upstream tank is a round tank. The area of upstream tank including the area of the dump is 4.75 m^2, given the diameter of the round tank 2.46 m. The area of the dump is 0.64 m^2. To sum up, the net area of the upstream tank is 4.11m^2.

The height difference of upstream tank

With regards to the measurement of height difference, it has been taken by means of a level water gauge, exclusively for the upstream tank. Owing to considering the flow volume with respect to flow over the dump to the upstream tank, the calibration has not initiated until the water height reached the value of 12.15 cm, instead of 0 cm. Nevertheless, it is noticed that tremendous differences to water height for calibration is inappropriate considering the constant supply of discharge from the upstream tank.

The evaluations made up of six different value of discharge have been made, given the height difference of water height, and thus corresponding volume can be obtained. Six different values of discharge used in the experiments for calibration is 1, 3, 5, 10, 15, and 20 l/s, separately. It is found that based on the first two assessment of flow discharge, the lower values of water height are not appropriate for such calibration.

Discharge (l/s)	Water height (cm)	Time (s)	Volume (m^3)	Calculated discharge (l/s)	average discharge (l/s)
1	12.15	26	-	-	1.02
	14.85	137	0.11	1	
	17.6	241	0.22	1.04	
3	12.15	26	-	-	2.89
	15	67	0.12	2.86	
	18.4	114	0.26	2.92	
5	12.15	20	-	-	4.74
	15.15	46	0.12	4.75	
	20.1	89	0.33	4.74	
10	12.15	17.2	-	-	10.03
	15.1	29.3	0.12	10.03	
	19.9	49	0.32	10.02	

	24.3	67	0.5	10.03	
15	12.15	16.8	-	-	15.19
	13.8	21	0.07	16.16	
	19.4	37	0.3	14.76	
	26.1	56	0.57	14.64	
20	12.15	13.9	-	-	19.67
	27	45	0.61	19.64	
	30.4	52	0.75	19.7	

Table 4-3 The calculated flow rate by means of volumetric measurement

4.2.5 Comparison between three kinds of flow rate measurements

The comparison regarding flow-rate measurement made by three different kinds of method has been shown in Table 4-6. Furthermore, the comparisons between the measurement of flowmeters and rectangular weir has been shown in Figure 4-3. The red line represents the measurement taken by rectangular weir, whereas the blue lines expresses measurement by electromagnetic flowmeters. When it comes to evaluation of performance, the coefficient of liner regression for two datasets, is 0.9998 and 0.9999, corresponding to measurement made by rectangular weir and electromagnetic flowmeters, respectively.

Discharge (l/s)	**Flowmeters (l/s)**	**Volumetric measurement (l/s)**	**Rectangular weir (l/s)**
1	0.99	1.02	1.06
3	2.92	2.89	2.88
5	4.85	4.74	4.77
10	10.15	10.03	10.27
15	14.93	15.19	15.24
20	19.74	19.67	20.1

Table 4-4 The comparison of three kinds of flow rate measurements

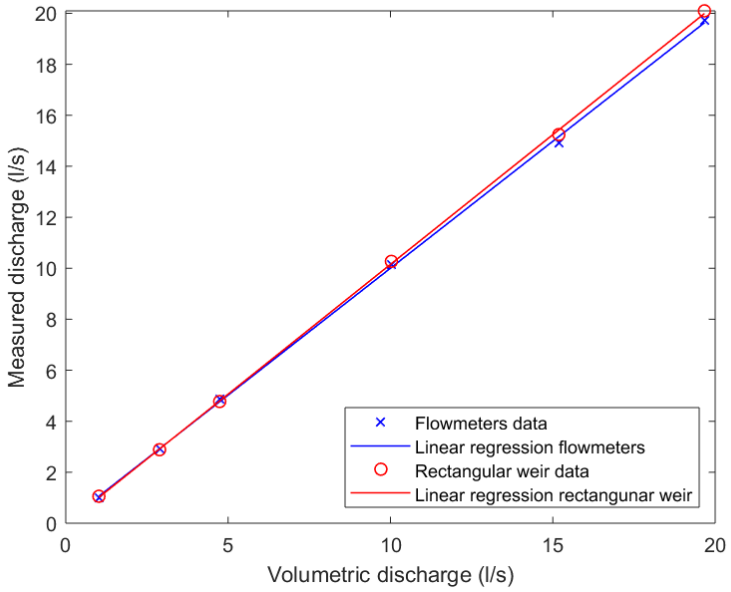

Figure 4-3 distribution of measured discharge as a function of volumetric discharge

4.2.6 Velocity measurement

Accurate velocities are essential to determine the threshold condition of incipient motion. For the experimental analysis, the velocities measurement has been measured with the use of Acoustic Doppler Velocimeter, as known as ADV (Figure 4-4). The stem of ADV is connected to the probe head, which consists of four acoustic receivers and an acoustic emitter (Figure 4-5). In addition, the stem is attached by a flexible cable to the signal-conditioning module which contains analog electronics for detection and amplification to acoustic signals.

The principle of ADV is based on Doppler effect. The emitter sends an acoustic ultrasound signal, traveling through the water and then reflected by the suspended particles in the water. Then the receiver captures and receives the echo, which is the superposition of several reflections from the particles.

In general, ADV is capable of measuring instantaneous velocities and accurate mean value of flow velocities in three-dimensions. For the experiments, the instantaneous velocities are selected instead of mean velocities profile. Various roughness geometries might result in the identical mean flow velocities, meaning the time-averaged characteristics of flow may be inadequate to describe the effects of roughness on flow characteristics. Therefore, incipient motion criteria based on time-averaged flow properties may not predict sediment transport appropriately.

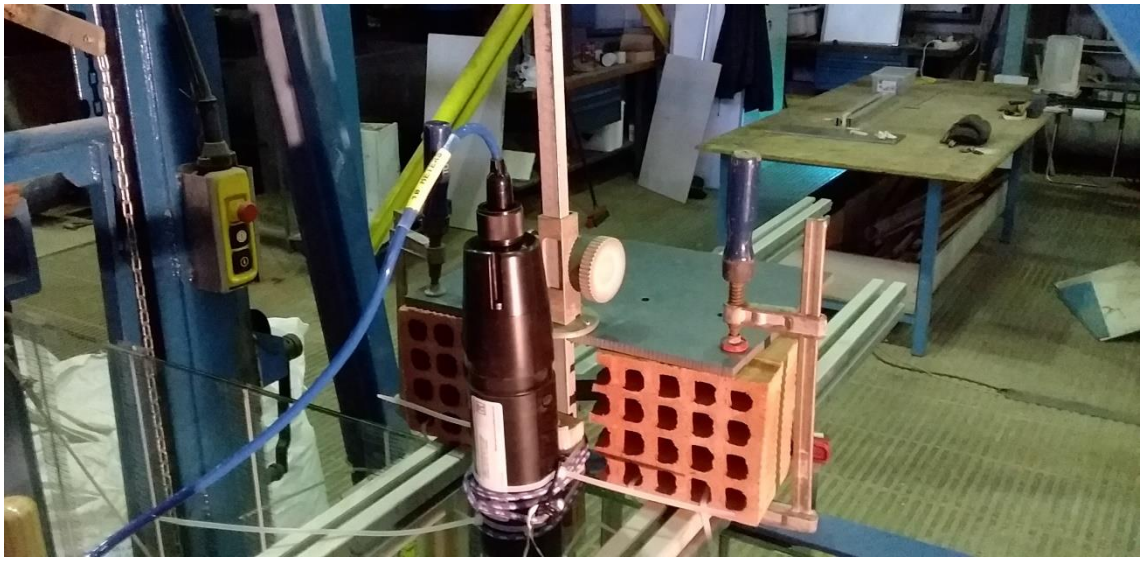

Figure 4-4 Acoustic Doppler Velocimeter

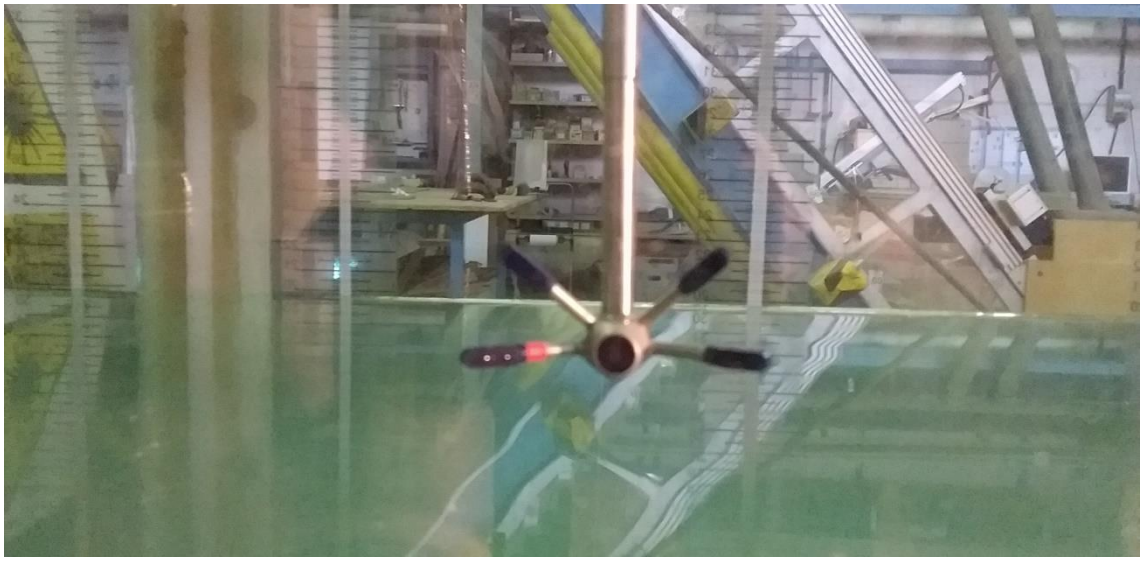

Figure 4-5 The probe head part of Acoustic Doppler Velocimeter

4.3 Characteristics of the materials

4.3.1 Filtration of sediment grains

In general, the sediments materials conducted for the experiments are crushed gravels. Nonetheless, prior to the experiment, those sediment grains were mixed together regardless of their size. Thus, to reclassify the sediment grains depending on the diameter size has to be done. First of all, unnecessary materials involved in those experimental materials such as plastic and clay balls have been removed. Secondly, the sediment materials have been sieved and reclassified based on the size of diameter by utilizing the grid mesh.

4.3.2 Diameter of the sediment grains

For the experiments, two meshes with different size have been applied, whose grids are 16mm*16mm, and 13mm*13mm. After the filtration, the sediment grains have been reclassified, whose median diameter are assumed to be 14.5mm. According to definition of Wentworth scale, while the median diameter of grain ranges from 16mm to 8mm, it is classified as medium gravel.

The reasons in favour of sediment grains based on the size of diameter are explained below. Firstly, one is the restrictions to laboratory facilities. It is related to maximum discharge rate approximately equal to 50 l/s. In general, to reach the threshold of motion, sediment grains with bigger size require higher discharge rate. Therefore, it is appropriate to select the diameter of sediment depends on the limitation. Secondly, as previous mentioned in chapter one, one of the objectives in the thesis aims to examine the Shields parameter in Shields diagram. For example, at the edge of the horizontal line described in the Shields diagram, the Reynold number is approximately 200, which corresponds to the size of sediment grains equals to 4 mm. Thus, to examine the Shields parameter, it is necessary to choose the sediment grains whose median diameter are bigger than 4 mm. In conclusion, the selection for size of diameter has to overcome these two restrictions mentioned above, and the size of diameter ranging from 16mm to 13mm is reasonable.

4.4 Experimental design

4.4.1 Assumption of experiments

For experimental analysis, certain conditions have been assumed. Firstly, the experimental sediment grains are considered non-cohesive. Despite of the difference of the diameter made by each particles, the median diameter of experimental sediments is assumed to be 14.5mm. Secondly, the flow is regarded as uniform, meaning the flow depth, water area, velocity, and discharge remains constant in every section of the channel.

4.4.2 The placement of sediment materials

As previously mentioned, channel is 9 meters long, divided into 40 sections. Each section is associated with the graduation scale labelled at the side wall used for the measurement of the water depth.

The materials used for carrying out the experiments are rounded gravels. The placement of rounded gravels ranges from section1 till section 31, and the height made up of those rounded gravels is 15cm. The rest of the sections act as the energy dissipation.

Among these sections, the section 12 (Figure 4-6) is identified as the test area to observe the threshold of movement. Quantities of sediments grains were painted beforehand, and were placed in this region, representing the indicator to examine the incipient motion.

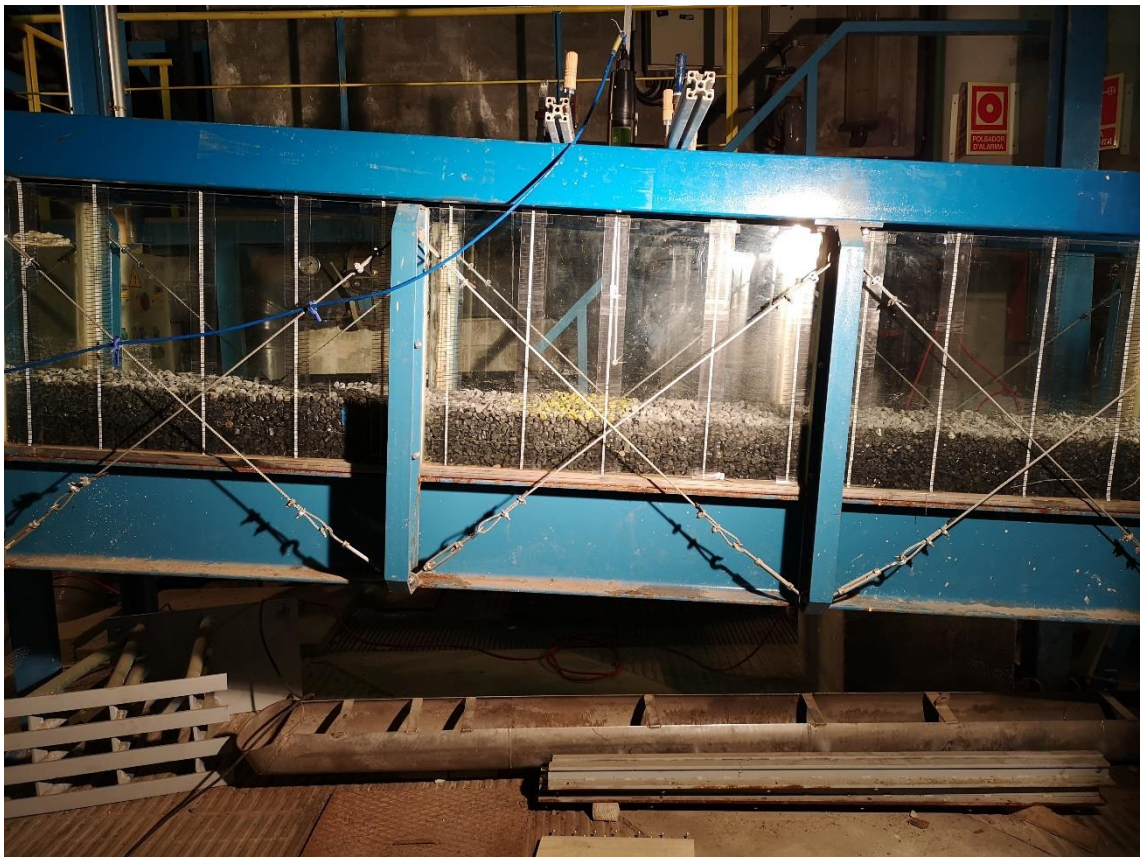

Figure 4-6 Test area with painted sediments and ADV

4.4.3 The placement of ADV

Inside the hydraulic channel, a test area is defined, serving as an indicator to determine the threshold of movement. The ADV device is placed in the centre between section 11 and section 12 (Figure 4-6). Above the channel, the ADV is access to the fixtures which enables to manage its position with the reference of graduation scale. Not until the sediments are in motion did ADV start to move downward until below the water surface to investigate velocity profile. The duration of velocity profile collection lasts for approximately 5 minutes.

4.5 Experimental procedure

4.5.1 Setting up the slope

When the experimental preparation is completed, next step is to set up the channel slope for the experiment. The slope set-up is managed by the automatic controller in charge of inclination angle of the channel. To further record the slope angle, the controller is equipped with a graduated scale which enables to indicate the slope.

4.5.2 Activation of pump

All experiments were performed under uniform flow conditions. Nevertheless, in reality, it is challenging to maintain such condition during the execution period. Despite of it, something still can be achieved. For example, once the pump is activated, it is necessary to set up the minimum flow rate until the sediment grains are fully submerged. Since a sudden increase in discharge is prone to the unexcepted incipient motion, operating the flow rate to at the minimum level is appropriate.

As soon as the sediment grains are submerged, the flow rate measurement as well as water depth measurement in terms of infiltration has been taken. The detail is illustrated in the next section.

4.5.3 The measurement of infiltration discharge

As mention above, once the sediment grains are fully submerged, recording the discharge made by infiltration is essential. The flow-rate when reaching the threshold of motion is separated from the flow-rate due to the infiltration.

In general, there are two methods to measure the infiltration discharge. One is by means of magnetic flowmeter, and the other is the application made by rectangular weir, using the piezometer as the reference. Once the recording is done, the flow rate is increased gradually until reaching the desired discharge.

4.5.4 Observation of incipient motion

Once the experiments are initiated, the flow-rate remains minimum until the sediment grains are fully submerged. Then when strengthening the flow rate, it is visible that a few sediments grains are involved in the rolling, even at the edge of threshold of motion (Figure 4-7). Nevertheless, there is no universal definition to determining threshold of movement since the threshold of movement is very subjective. Thus, conducting the experiments in the same criteria is so important that the following experiments could repeat the same procedure.

The principle put into practice in the experiments to define the incipient motion is based on the visualization of sediment materials. To be more specific, prior to the experiments, a small portion of sediments have been painted, acting as an indicator in test section. In general, the criteria to determine incipient motion is based on the ratio of number of sediment particles displacements to total sediment particles. When the sediment particle no longer stayed its own position, it was called particle displacement. Once the ratio of particle displacements reached approximately 10 percentage with regards to test section area, it is defined as the threshold condition of sediment movement. Figure 4-8 represents the movement of painted sediment grains after the experiment.

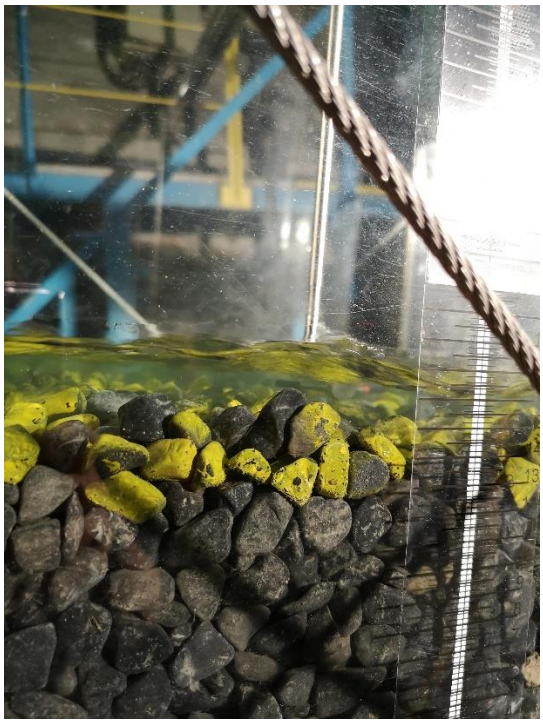

Figure 4-7 The sediment movement during the experiment

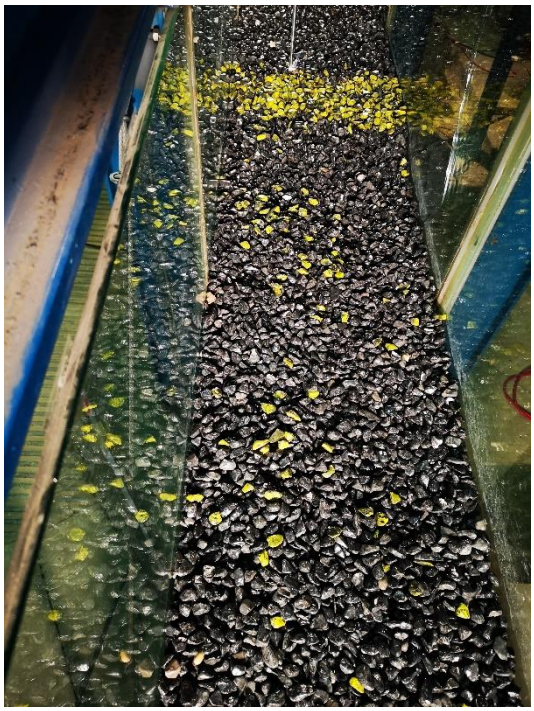

Figure 4-8 The sediment movement after the experiment

4.5.5 The recording of velocity profile (ADV measurement)

The investigation of the velocity profile is followed by the determination of threshold of motion, which means at least 10 percentage of painted sediment grains are set in motion during the 10 minutes examination period. The investigation of velocity profile taken by ADV as well as hydrodynamic data is under the flow-rate corresponding to the incipient motion.

If the threshold of motion is determined, the ADV data collection starts. For the thesis, the velocity profile in terms of x-direction as well as its corresponding depth is recorded. The y-direction, and of velocity profile at y-direction, and z-direction are excluded since

the x-direction represents direction of flow for the experiments. When such investigation is finished, the flow rate is reduced progressively until shutting the pump down.

4.6 Summary

In chapter four, the related laboratory facilities, experimental measurement, and experimental procedure have been presented. Still, a few things need to be carefully examined. First of all, once the pump was activated, the discharge into the channel was supposed to be maintained minimum until the sediment particles were fully infiltrated. To ensure the flow-rate not being able to increase suddenly is essential since even at the minimum flow rate the sediment motion might occur owing to the turbulence of the flow. Secondly, significant sediment transport resulted from the interference by ADV during the velocities profile investigation occurred. It has been observed that when the ADV was placed below the flow surface, the streamflow was likely to be altered, further initiating sediment transport, and thus erosion. Thirdly, during the experiments, it has been noticeable that as long as the channel was discharged, instability of particles caused by flow was observed despite of standing still in the own position. Some of the particles were found to be in motion, while others remained vibration. This may be resulted from the forces between each particle, which are not considered in the conceptual method. Due to the visualization of threshold motion, the subjective interpretation is unavoidable.

Chapter 5. Results

5.1 Introduction

In chapter four, the related experimental set-up such as laboratory facilities, flow measurement was clearly introduced. Subsequently, the experimental data has obtained from visualization of threshold of motion been presented in this chapter. Section 5.2.1 presents main hydraulic variables derived from experimental data. Section 5.2.2 presents the calibration of conceptual method shown in section 3.4. Section 5.2.3 presents the normalization to flow depth. Section 5.2.4 follows the form of Shields diagram by means of the data obtained from experimental investigation. Section 5.2.5 describes the flow resistance coefficient and constructs the relationship as a result of roughness (D_{50}/d). Section 5.2.6 introduces the relative roughness.

5.2 Experimental results

5.2.1 Experimental data as well as hydraulic variables

Results obtained from the experimental investigation, such as flow rate (Q), flow depth (d), and mean velocity (U), as well as the related hydraulic variables, are presented below in Table 5-1. The shear velocity (u*) is obtained from the Eq. 3-20; The Froude number is related to Eq. 3-18; The bed shear stress (τ_0), and dimensionless shear stress (τ^*) are derived from Eq. 3-2, and Eq. 3-7, respectively. Last but not least, the Reynold number arises from the Eq. 3-3.

Figure 5-1 shows the trend regarding the flow rate (Q) and the flow depth (d). Each point is reference with inclination angle (α). The flow rate is highly correlated to flow depth. In addition, it implies the inverse relationship between slope angle and flow depth. As the slope angle increases, the flow rate decreases in terms of decreasing flow depth under threshold condition.

Slope angle (α) (%)	Flow rate (Q) (l/s)	Flow depth (d) (m)	Mean velocity (U) (m/s)	Shear velocity (u*) (m/s)	Froude number (Fr)	Bed shear stress (τ_0) (N/m^2)	Dimensionless shear stress (τ^*)	Particle Reynold number (Re*)
3.68	18.84	0.049	0.95	0.12	1.37	14.32	0.098	1735.30
3.89	17.53	0.044	1.00	0.12	1.53	13.69	0.099	1696.58
5.01	14.96	0.039	0.96	0.13	1.55	16.02	0.124	1835.04
6.00	11.56	0.034	0.85	0.13	1.48	17.01	0.143	1891.01
6.00	12.26	0.032	0.96	0.13	1.71	16.21	0.140	1846.01
6.04	11.75	0.033	0.89	0.13	1.56	16.81	0.143	1879.80
7.00	9.37	0.025	0.92	0.12	1.60	15.47	0.154	1803.61
7.00	7.48	0.024	0.78	0.12	1.84	14.72	0.151	1759.29
8.01	6.35	0.023	0.69	0.13	1.44	16.25	0.172	1848.49
8.92	6.91	0.022	0.79	0.13	1.70	17.22	0.190	1902.89
8.92	6.09	0.022	0.70	0.13	1.53	17.06	0.189	1893.84
10.66	4.72	0.018	0.67	0.13	1.63	16.73	0.216	1875.50

Table 5-1 Experimental results and related hydraulic variables obtained from the experiments

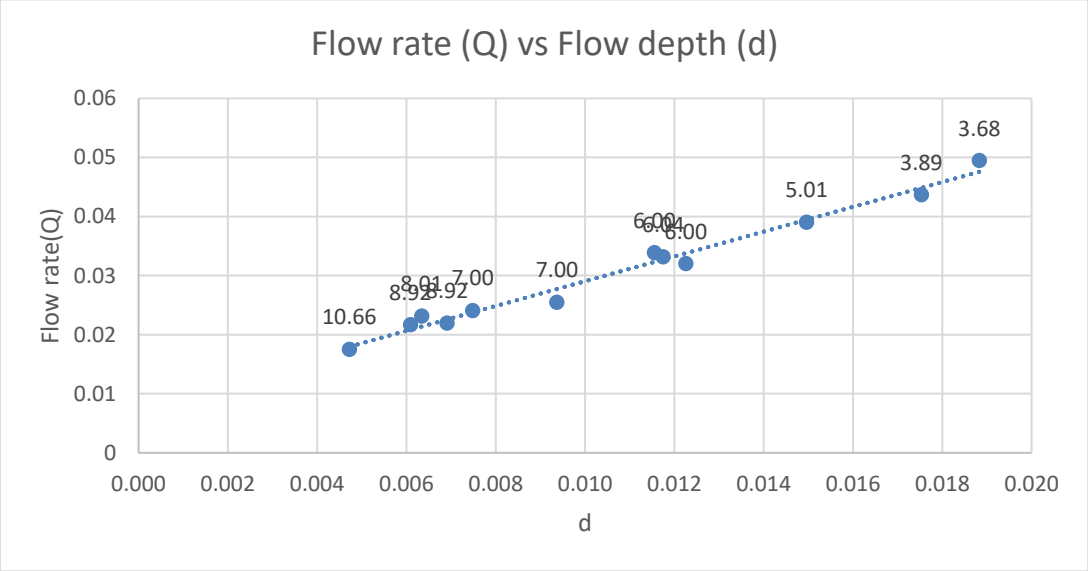

Figure 5-1 Distribution of flow rate as a function of flow depth

5.2.2 The equation derived from equilibrium of force analysis

In section 3.4, a conceptual method (Eq. 3-17) to describe the force balance on non-horizontal surface has been presented. By observing such equation, it is found that all of the variables were known prior to experimental investigation, except bed shear stress (τ_0). Once conducting the experiments, it is able to calculate the discharge and flow depth based on the Manning equation as well as the equilibrium of force analysis, as presented in Table 5-2. For the threshold of movement, generally both experimental value of flow rate and flow depth were overestimated, comparing with the estimated values.

Figure 5-2 depicts the relationship of conceptual equation derived from Eq. 3-17, where the x-axis represents the value of $((\mathrm{Ss}-1)\cos\theta\tan\varphi - Ss\sin\theta)$; y-axis is $\tau_0\left(\frac{1}{2}+\frac{1}{2}\tan\varphi\right)/\frac{2}{3}\gamma D$. As it can be seen, it represents an inverse relationship, indicating that the linear regression analysis is improper. Instead, a polynomic trend is more appropriate with greater value of R^2. Despite of R^2 value, it implies the low correlation for the conceptual method, which might arise from the simplification for the configuration of cross-section.

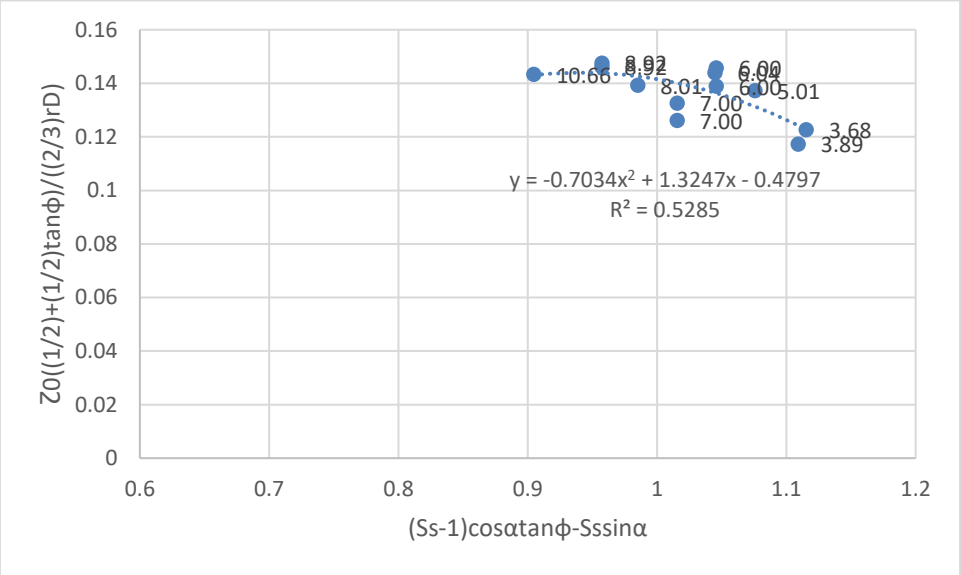

Figure 5-2 The distribution of $\tau_0\left(\frac{1}{2}+\frac{1}{2}\tan\varphi\right)/\frac{2}{3}\gamma D$ as a function of $((\mathrm{Ss}-1)\cos\theta\tan\varphi - Ss\sin\theta)$

Slope angle (α) (%)	Q(observed) (m^3/s)	Q(estimated) (m^3/s)	d(m) (observed)	d(m) (estimated)
3.68	0.01884	0.01885	0.0495	0.0495
3.89	0.01753	0.01958	0.0437	0.0469
5.01	0.01496	0.01378	0.0390	0.0370
6.00	0.01156	0.01021	0.0338	0.0313
6.00	0.01226	0.01021	0.0320	0.0313
6.04	0.01175	0.01062	0.0332	0.0311
7.00	0.00748	0.00900	0.0241	0.0271
7.00	0.00937	0.00900	0.0255	0.0271
8.01	0.00635	0.00662	0.0232	0.0237
8.92	0.00691	0.00653	0.0219	0.0212
8.92	0.00609	0.00653	0.0217	0.0212
10.66	0.00472	0.00463	0.0175	0.0173

Table 5-2 The estimated value versus the observed value regarding flow depth and discharge

5.2.3 Normalization to flow depth

It is noticeable that difference of flow depth which arises from the visual observation might result in significant difference in hydraulic parameters. For example, sensitivity analysis has been made by putting a sensitive value (σ=0.5mm) into flow depth (d) and discharge (Q), to examine difference between new Froude number and initial Froud number. According to Figure 5-3, it is observable that once the slope angle increases, the impact on Froude number owing to the sensitive value are more significant. In response to such issue, the value of water depth derived from experiments has been normalized, aiming at minimizing the effect made by visualization.

The method for normalization was collecting the flow rate data as well as the flow depth data each time when changing the flow discharge. Once discharge rate increased, the flow depth was recorded. Such flow depth data as a function of flow rate was normalized by means of the exponential curve, and thus normalized flow depth (h^+) was created. Figure 5-4 suggests the direct proportional relationship between normalized flow depth and initial flow depth.

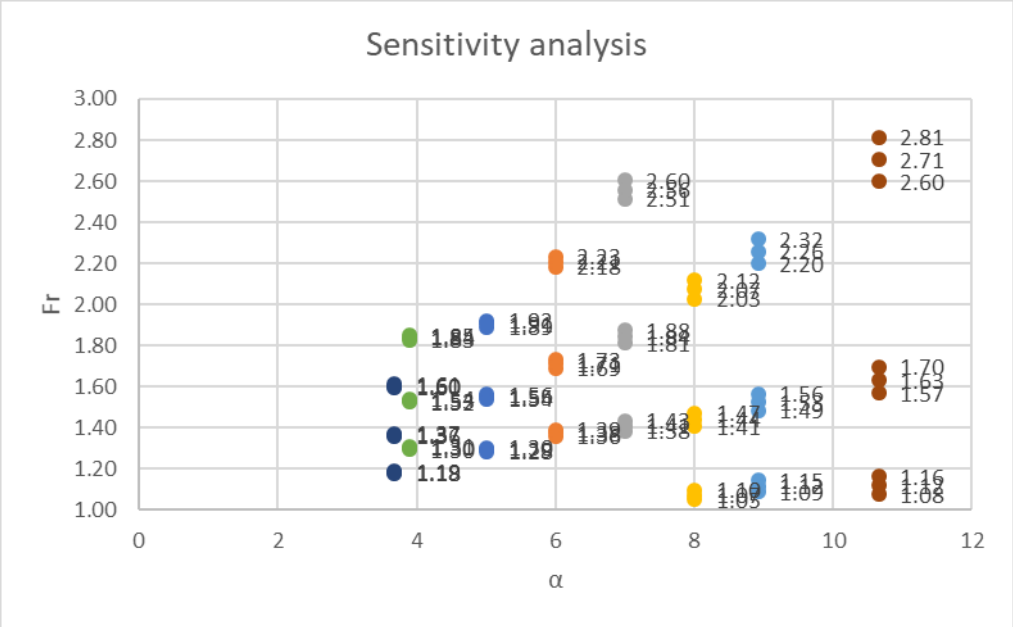

Figure 5-3 Sensitivity analysis regarding Froude number considering the sensitive value (σ)

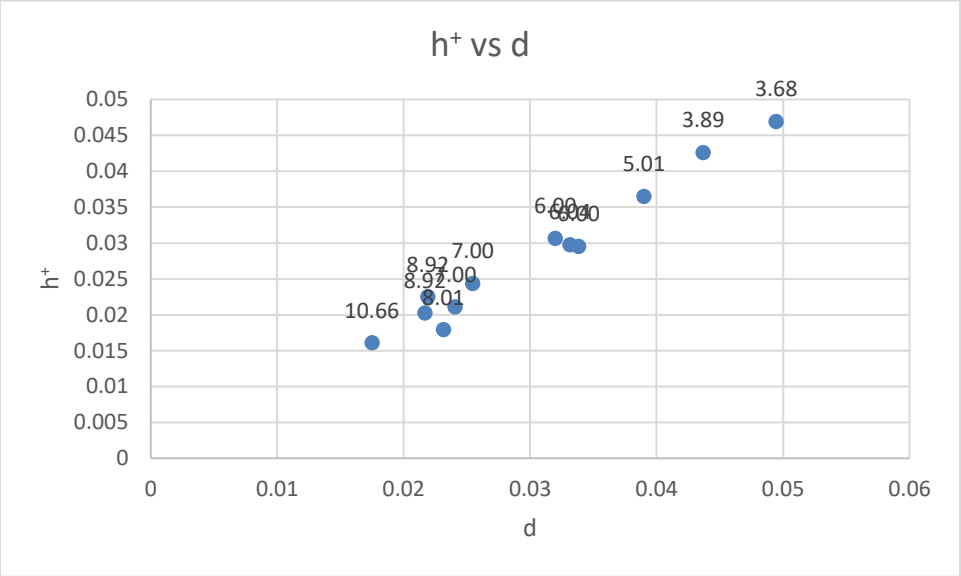

Figure 5-4 Distribution of normalized depth as a function of flow depth

5.2.4 Evaluation of dimensionless shear stress

Figure 5-5 depicts the dimensionless shear stress as a function of particle Reynold number as the form of Shields diagram. Each value is labelled as the inclination angle (%). It is found that the dimensionless shear stress is proportional to the slope angle, whereas the value of Reynold number at the condition of inclination angle 5% to 6 % is higher than expected, which implies over the threshold of movement.

With regards to the normalized flow depth, the dimensionless shear stress as well as particle Reynold number also show a trend of proportionality (Figure 5-6). Despite of proportional relationship, underestimation of the threshold of motion is found at the condition of 7% and 8.01%.

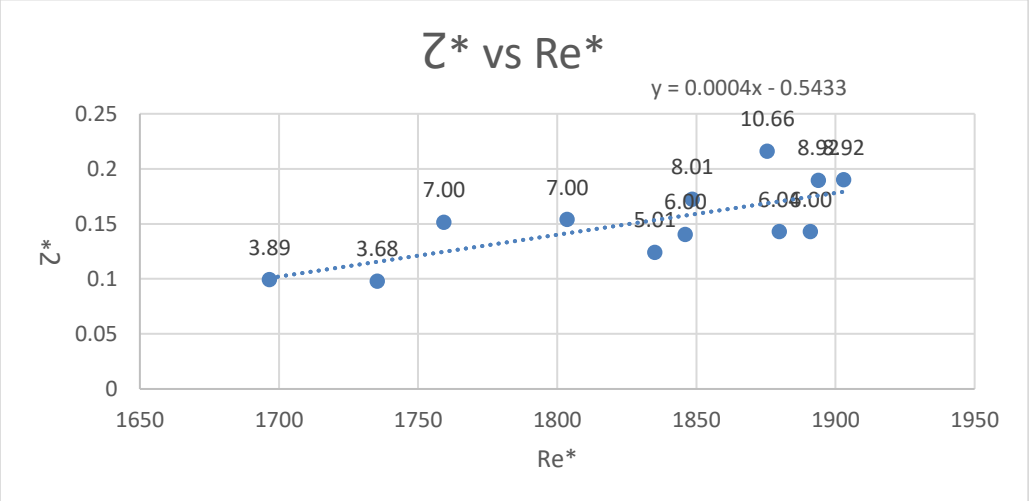

Figure 5-5 Distribution of dimensionless shear stress as a function of Reynold number

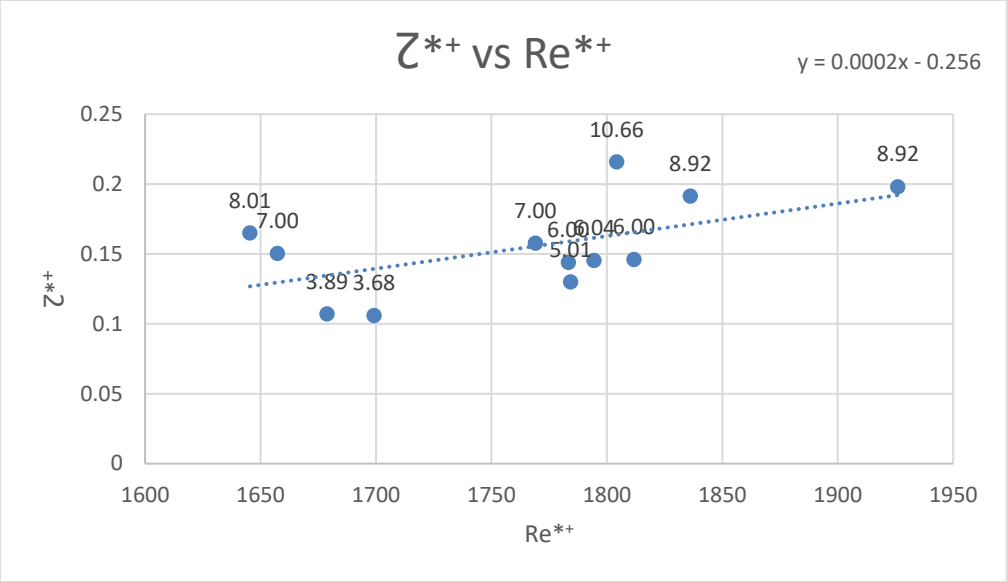

Figure 5-6 Distribution of dimensionless shear stress as a function of Reynold number derived from normalized depth

5.2.5 Flow resistance coefficient

The Manning coefficient (n) and friction coefficient (C_f) derived from hydraulic variables are shown the Table 5-3. Figure 5-7 depicts the Manning coefficient in terms of D_{50}/d. D_{50}/d is inverse ratio of relative submergence (d/D_{50}), which is associated with the roughness. It shows that the Manning coefficient is proportional to the ratio D_{50}/d, with regards to the rising inclination angle (θ). Figure 5-8 describes the friction coefficient as a function of D_{50}/d. Likewise, it shows a trend of proportionality with respect to D_{50}/d.

In hydraulic engineering, the Manning coefficient is a coefficient, representing the friction applied to the flow by the channel. According to the Figure 5-7, at the condition of growing slope, the ratio D_{50}/d is on the rise, which implies the increase in the Manning coefficient.

Secondly, it is known that the shear velocity (u^*) is associated with the friction brought by the bed shear stress (τ_0). Based on Figure 5-8, at the threshold of movement, as the slope increases, the bed shear stress increases accordingly, suggesting higher friction coefficient.

Slope angle (%)	n (Manning coefficient)	C_f (friction coefficient)	D_{50}/h
3.68	0.023	0.016	0.29
3.89	0.021	0.014	0.33

5.01	0.024	0.017	0.37
6.00	0.027	0.023	0.43
6.00	0.023	0.018	0.45
6.04	0.026	0.021	0.44
7.00	0.023	0.024	0.60
7.00	0.026	0.018	0.57
8.01	0.031	0.035	0.63
8.92	0.028	0.028	0.66
8.92	0.031	0.035	0.67
10.66	0.031	0.037	0.83

Table 5-3 Flow resistance coefficient values

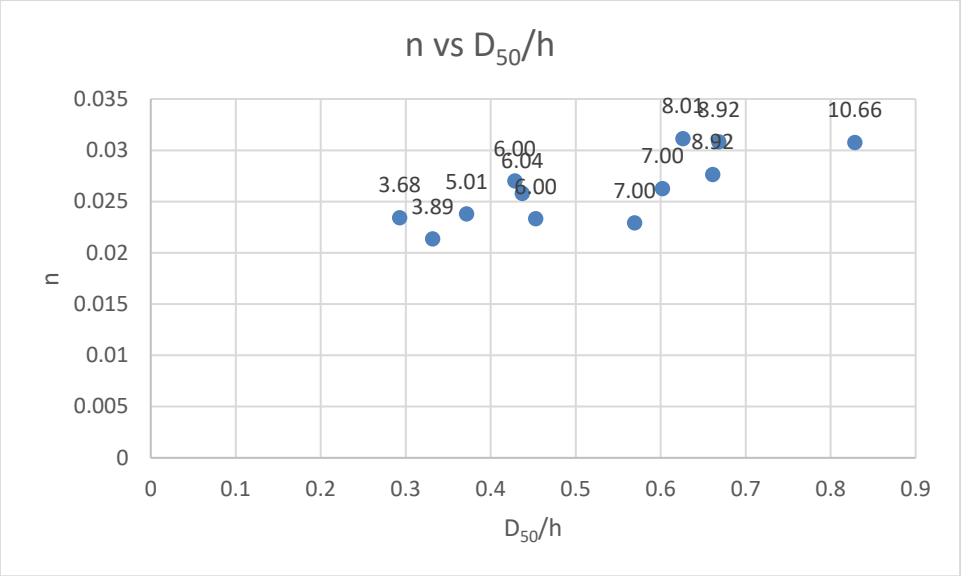

Figure 5-7 Distribution of Manning coefficient as a function of relative roughness

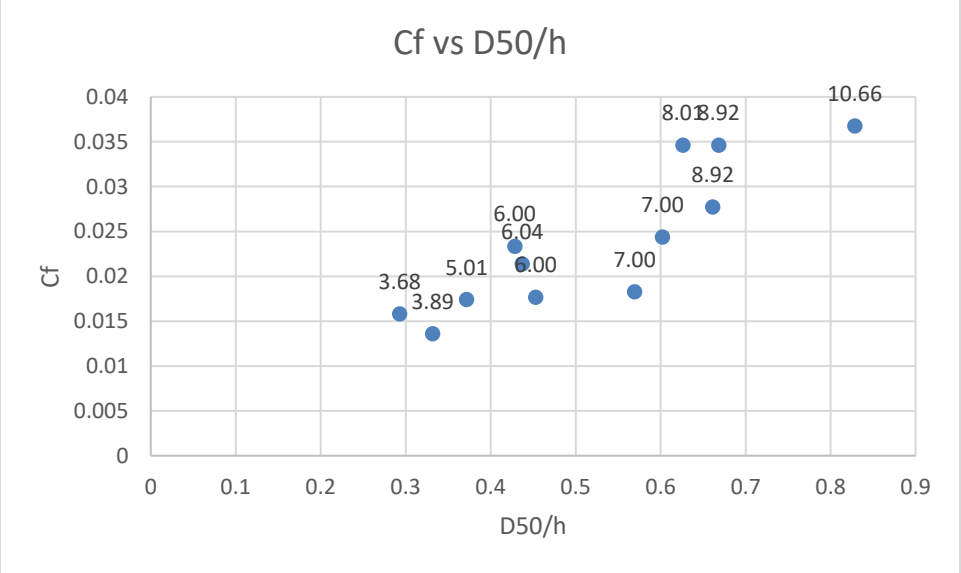

Figure 5-8 Distribution of friction coefficient as a function of relative roughness

5.2.6 Relative roughness height

The relative roughness height (k_s) and slope angle (%) has been shown in Table 5-3. The average of relative roughness was approximately 7mm, equal to one half to the particle diameter (14.5mm).

K_s (m)	α (%)
0.00769	3.68
0.00659	3.89
0.00748	5.01
0.00383	6.00
0.00075	6.00
0.00629	6.04
-	7.00
0.00370	7.00
0.00204	8.01
0.00400	8.92
0.00342	8.92
0.03076	10.66
$0.00696_{(average)}$	

Table 5-4 relative roughness height in terms of slope angle

5.3 Summary

In this chapter, experimental data as well as its related hydraulic variables have been presented.

The experimental results have been applied to address the slope effect on dimensionless shear stress by means of application of Shields diagram, as a function of Reynold number. It indicates a roughly increase trend as the slope angle rises. In addition, the normalization to flow depth has been done. However, the occurrences of deviation from the results are found in the Shields diagram. The overestimation as well as underestimation might result from the subjectivity to visualization of threshold of motion

Friction coefficient as well as Manning coefficient as a function of relative roughness have been examined. For the former, at the threshold of motion, the friction made by bed shear stress increases corresponding to growing slope angle. Thus, it is reasonable that friction coefficient increases. For the latter, the decreases in flow depth suggest the higher roughness, and thus higher Manning coefficient.

Chapter 6. Discussion

6.1 The difference made by slope on threshold of motion

6.1.1 Investigation by means of Shields diagram

As mentioned earlier, one of the objectives is to compare the flume data obtained from experimental investigation with Shields diagram, whereas the initial Shields diagram did not consider the slope angle. As seen Figure 3-1, at the condition of horizontal surface, when the Reynold number is roughly greater than 10^3, the Shields parameter remains constant with a value 0.056.

The comparison between horizontal surface between non-horizontal surface has been presented in Figure 6-1. The experimental data regarding dimensionless shear stress as a function of Reynold number obtained from Figure 5-5 has been plotted as red points. All of the experimental data (from inclination angle equals to 3.68(%) till 10.66 (%)) corresponds to Reynold number between$1.7x10^3$ and $1.9x10^3$. In addition, the extrapolation line derived from such red points has been shown in Figure 6-1, as a representative of red line. It is concluded that instead of remaining constant at the condition of horizontal surface, the dimensionless shear stress increases approximately proportionally as a result of increasing slope angle. Also, the extrapolation line implies that once the Reynold number is greater than $1.498x10^3$, the dimensionless shear stress no longer equals to 0.056, and thus increases roughly proportionally.

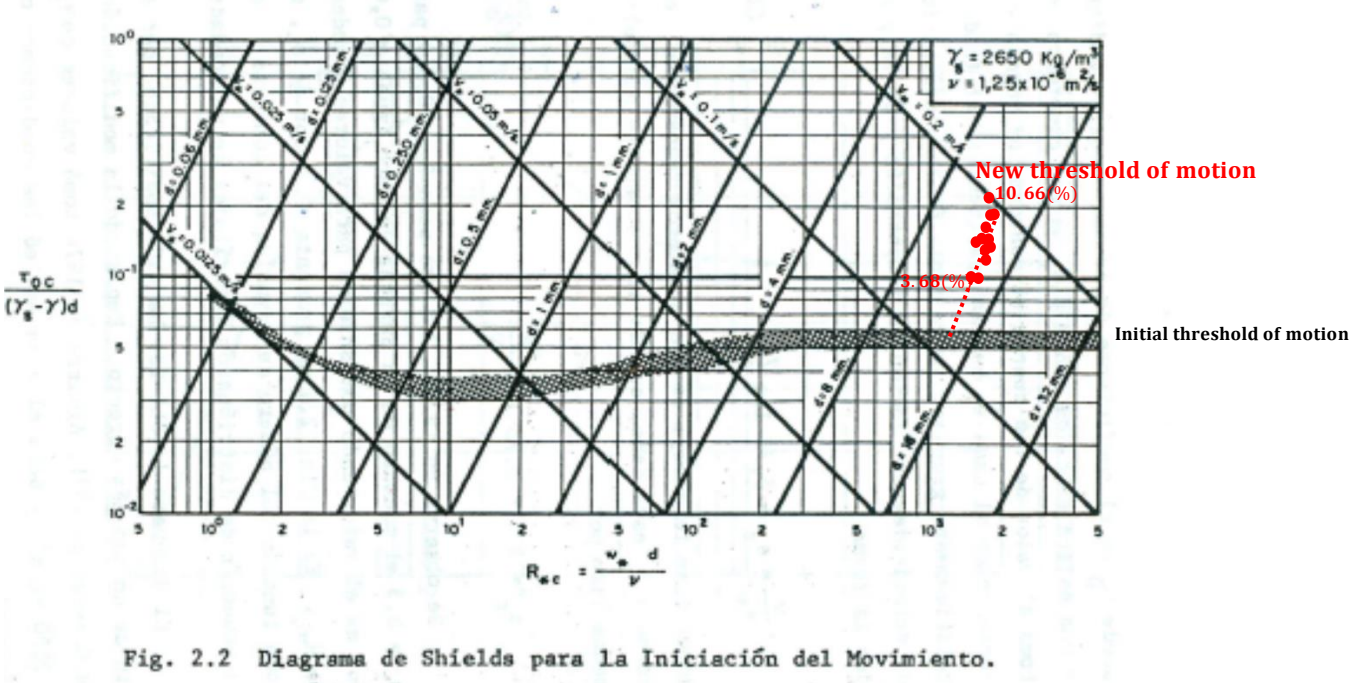

Fig. 2.2 Diagrama de Shields para la Iniciación del Movimiento.

Figure 6-1 Representation of experimental results regarding threshold of motion on initial Shields diagram

6.1.2 Analysis of resultant forces with respect to the slope effect

In Chapter 3, Eq. 3-7 defines the dimensionless shear stress, which is composed of the ratio of destabilizing force to stabilizing force acting on a sediment grain. Figure 6-2 indicates the trend of the stabilizing forces, which are buoyant force (B), lift force (F_L), and the component of gravity force ($w_s \cos\alpha$) as a function as inclination angle; whereas Figure 6-3 shows the destabilizing forces, composed of the component of gravity force ($w_s \sin\alpha$), and drag force (F_D) act as the function of inclination angle. It is observable that all of the forces do not differ significantly, except the component of gravity force ($w_s \sin\alpha$) increases significantly. Therefore, it is concluded that when the inclination angle increases, the value of dimensionless shear stress increases accordingly due to the growing destabilizing force.

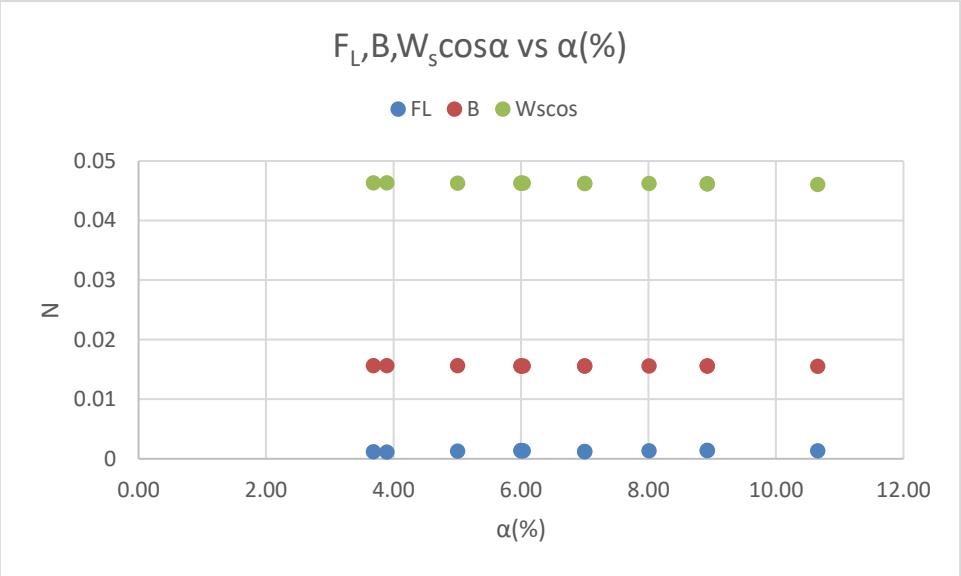

Figure 6-2 Distribution of stabilizing forces as a function of inclination angle (α)

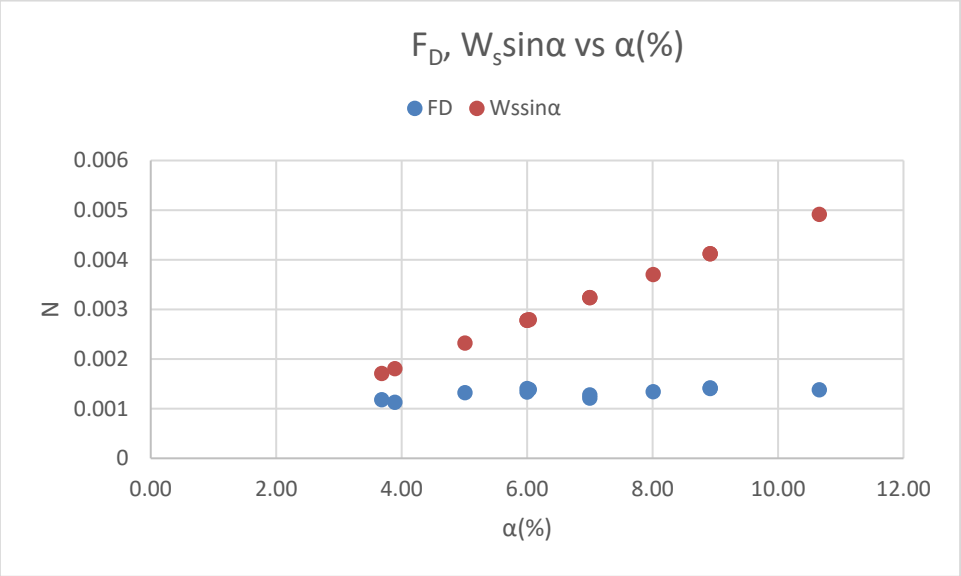

Figure 6-3 Distribution of destabilizing forces as a function of inclination angle (α)

6.2 Implication to flood risk assessment

In reality, regarding the flood in high mountain rivers, it is related to the behaviour of sediment transport and the concept of threshold of motion. To be more specific, in terms of high mountain rivers, when the flow reaches to critical condition, meaning Froude number equal to 1, the threshold of motion was initiated, causing erosion. The flow intends to maintain the critical condition, and thus the avulsion occurs, altering the geometry. Once the avulsion happens, the cross section of channel becomes wider and the flow depth increases (seen in Figure 6-5). At the same time, the sediments are trapped, forming the deposition. Thus, due to such deposition, it causes high water level in the upstream of river as well as flood.

The thesis provides some hints to determine the threshold of movement in high mountain rivers. In response to the situation above, the flood risk assessment has to be reconsidered as a result of slope effect on the threshold of motion. However, regarding the flood risk assessment, several issues still needs to be addressed. First of all, for the thesis, it is found that the manning coefficient does not remain constant with regards to variation to slope angle (seen in Table 5-2). Such value has a tremendous impact on the evaluation on hydraulic variables, and thus flow depth. Secondly, how the channel configuration, flow depth, and floods are quantitatively affected need more investigation.

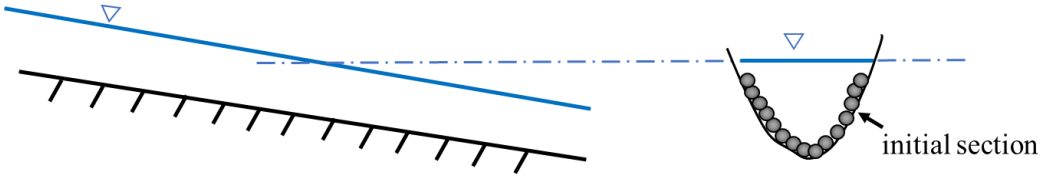

Figure 6-4 schematic diagram of initial cross section of channel

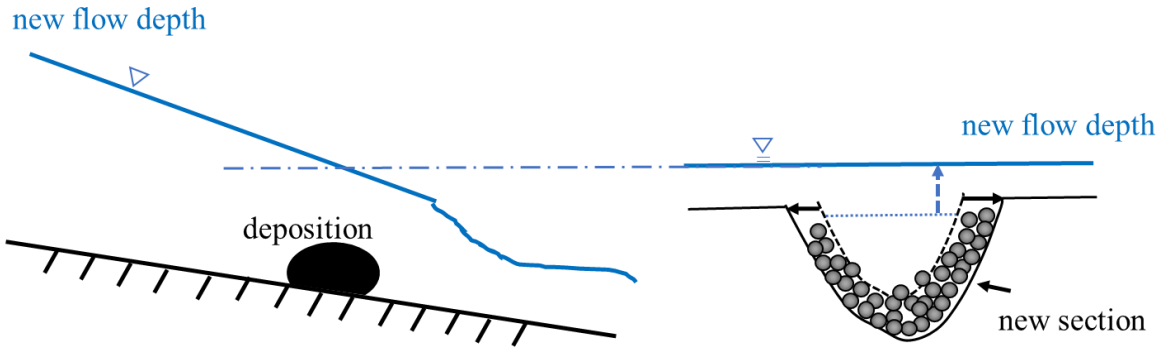

Figure 6-5 schematic diagram of cross section of channel when avulsion happens

6.3 Limitations

6.3.1 Subjectivity due to visualization of threshold of motion

Due to the fact that there is no general definition of threshold of motion with respect to the experimental investigation, therefore for the thesis it was determined by means of the visualization of sediment entrainment. However, in terms of visualization method, it is unlikely to count the same number of sediment particles for each experimental analysis. The overestimation as well as underestimation of threshold of motion was found in the Shields diagram addressing slope effect (Figure 5-4). The subjective judgement owing to the visualization probably results in the deviation of threshold of motion.

6.3.2 Limitation due to the existing facilities

As shown in the Table5-1, all of the experiments were under the condition of supercritical condition, meaning the Froude number (Fr) greater than 1. In general, the thesis aims to reach the critical condition (Fr=1) for each experiment. Nonetheless, Due to the limitation of available facilities, the hydraulic channel is not able to be operated with higher flow rate with an eye to reaching the critical condition. Despite of being able to reach critical condition, the dimensionless shear stress shoes a trend of proportionality to the inclination angle.

6.3.3 Investigation of cross-section geometry

For the thesis, the conceptual method considered the configuration of the cross-section area to be rectangular. Nonetheless, due to its simplification, it requires further investigation. Consequently, the configuration of cross section of channel can be set up as triangle, trapezoid, or parabolic.

6.4 Summary

In this chapter, we have discussed the difference to the dimensionless shear stress between horizontal surface and non-horizontal surface. It is found that regarding slope effect, when the threshold of motion is initiated, the dimensionless shear stress does not remain constant 0.056 as Shields assumed. Instead, it starts to increase proportionally when particle Reynold number is approximately greater than $1.5x10^3$. It is concluded that the Shields diagram needs to be modified or at least requires further investigation with regards to the slope effect.

To realize the mechanism to such difference, we have analysed the resultant forces. As previously mentioned, by means of force analysis, the definition to the dimensionless shear stress is the ratio of destabilizing forces to stabilizing forces. Comparing with the horizontal situation, the difference comes from the influence from the component of gravity force. As the inclination angle increases, such force acts as increase in the destabilizing force; whereas other forces acting on the particle grain do not increase or decrease significantly. Thus, it is concluded that influence of slope or gravity force has an impact on the threshold of motion, and thus alters the value of dimensionless shear stress.

Nonetheless, the new dimensionless shear stress as a function of particle Reynold number presented in Figure 5-4 indicates the occurrence of overestimation. This might arise from the subjectivity in the threshold of motion. For experimental analysis, it was assumed the threshold condition is determined by means of visualization. Apparently, subjective judgement is unavoidable, resulting in the deviation to determination.

Chapter 7. Conclusion and Recommendation

7.1 Conclusion

Over the past decades, many efforts have been made to investigate the threshold of sediment movement. Shields diagram (1936) is the most common method to characterize such significant topic in hydraulic engineering. He assumed that the threshold of motion occurs when the dimensionless shear stress is greater than 0.056. In response, the formula to describe the threshold of motion as well as Shields parameter was proposed. Nevertheless, it did not take the slope effect into account.

For the thesis, the main objective is to assess threshold condition of sediment motion taking slope effect into account for sediment entrainment. This has been achieved by means of proposition of a conceptual method as well as the experimental investigation for data collection. For the former, the threshold of motion was identified by examining resultant forces acting on a grain lying on a non-horizontal slope. The latter was executed by means of conducting the experiments. Sediment particles for experimental analysis were placed inside a hydraulic open-channel, with manageable inclination angle as well as flow rate. The threshold condition of incipient motion was observed by means of visualization.

The experimental results suggest that the value of dimensionless shear stress is not constant when Re* is approximately greater than $1.5x10^3$. Instead, dimensionless shear stress increases as a result of growing inclination angle. In terms of force analysis, it is found that the component of gravity force plays a vital role in determining the value.

To sum up, after proposing the conceptual method and conducting the related experiments, the thesis is capable of taking slope effect into account to determine the threshold of motion as well as the value of dimensionless shear stress by means of force analysis. Such studies might give some hints to assess the threshold of motion in high mountain rivers with an eye to addressing the flood risk assessment.

Nonetheless, the thesis is subject to a few issues. First of all, there is no universal definition of threshold of motion for experimental analysis. Thus, subjective interpretation owing to visualization is unavoidable. Secondly, the conceptual method did not include the forces between particles, which implies its simplicity. Although the trends in qualitative way were noticed, there were some uncertainties that needs to be examined. Thirdly, all of experimental investigation is at the condition of supercritical (Fr >1), not

being able to reach to critical condition as the thesis assumed (Fr =1), owing to the limit condition of facilities.

7.2 Recommendation

During the development of the thesis, a few aspects could be improved in future. The present work could also be extended in some directions that will strengthen the findings of the current work. These are listed below:

- Investigate the configuration of the cross-section by replacing rectangular with triangle, or parabola.
- Propose the better criteria to determine the threshold of motion for experimental investigation.
- Improve the conceptual method to address equilibrium of force balance on the sediment entrainment developed in this thesis, such as considering the clamping forces between each sediment particle.

References

Allen, J.R.L. (1982). “Simple models for the shape and symmetry of tidal sand wave: (1) statically stable equilibrium forms.” Mar. Geol., Vol. 48, pp. 31-49.

Andrews, E. D., Entrainment of gravel from naturally sorted riverbed material, Geol. Soc. Am. Bull., 94, 1225-1231, 1983.

Ashworth, P. J., and R. I. Ferguson, Size-selective entrainment of bedload in gravel bed streams, Water Resour. es.2, 5, 627-634, 1989.

Ashworth, P. J., R. I. Ferguson, P.E. Ashmore, C. Paola, D. M. Powell, and K. L. Prestegaard, Measurements in a braided river chute and lobe, 2, Sorting of bed load during entrainment, transport, and deposition, Water Resour. Res.,2 8, 1887-1896,1 992.

Armanini, A., and C. Gregoretti (2005), Incipient sediment motion at high slopes in uniform flow condition, Water Resour. Res., 41, W12431, doi:10.1029/2005WR004001

Buffington, J.M. (1999). “The legend of A. F. Shields.” J. Hydraul. Eng., Vol. 125, No. 4, pp. 376-387.

Buffington, J.M. and Montgomery, D.R. (1997). “A systematic analysis of eight decades of incipient motion studies, with special reference to gravel-bedded rivers.” Wat. Resour. Res., Vol. 33, No. 8, pp. 1993-2029.

Carling, P. A., Threshold of coarse sediment transport in broad and narrow natural streams, Earth Surf. Processes Landforms, 8, 1-18, 1983.

Chiew, Y.M. and Parker, G. (1994b). “Incipient sediment motion on non-horizontal slopes.” J. Hydraul. Res., Vol. 32, No. 5

Christensen, B. A. (1995) Incipient Sediment Motion On Non-Horizontal Slopes, Journal of Hydraulic Research, 33:5, 725-730

Day, T. J., A study of the transport of graded sediments Rep. IT190, 10 pp., Hydraul. Res. Stn., Wallingford, U. K., 1980.

Dey, S. (2003). “Threshold of sediment motion on combined transverse and longitudinal sloping beds.” J. Hydraul. Res., Vol. 41, No. 4, pp. 405-415.

Dey, S. (1999). “Sediment threshold.” Appl. Math. Modelling, Vol. 23, No. 5, pp. 399-417.

Dey, S. and Debnath, K. (2000). “Influence of stream-wise bed slope on sediment threshold under stream flow.” J. Irrig. and Drain. Eng., Vol. 126, No. 4, pp. 255-263.

Diplas, P., Bedload transport in gravel-bed streams, J. Hydraul.Eng.,113, 277-292, 1987

Fernandez Luque, R. & Van Beek, R. (1976) Erosion and transport of bed-load sediment. J. Hydraul. Res. 14 (2), 127–144.

Gilbert, G. K., The transportation of d6bris by running water, U.S. Geol. Surv. Prof. Pap. 86, 263 pp., 1914.

Gregoretti, C. (2008), Inception sediment transport relationships at high slopes, J. Hydraul. Eng., 134(11), 1620–1629, doi:10.1061/(ASCE)0733-9429(2008)134:11(1620).

Hjulström, F., 1935. Study of the Morphological Activity of Rivers as Illustrated by the River Fyris Bulletin, vol. 25, Geological Institute of Upsala, Upsala, Sweden.

Howard, A.D. (1977). “Effect of slope on the threshold of motion and its application to orientation of wind ripples.” Bull. Geol. Soc. Am., Vol.88, pp. 853-856.

Iversen, J.D. and Rasmussen, K.R. (1994). “The effect of surface slope on saltation threshold.” Sedimentation, Vol. 41, pp. 721-728.

Jiang, Z., and P. K. Haft, Multiparticle simulation methods applied to the micromechanics of bed load transport, Water Resour. Res., 29, 399-412, 1993.

Keulegan, G. H. (1938), ‘Laws of Turbulent Flow in Open Channel’. U.S. National Bureau of Standards, Journal, 21(1151), 707-741

Kindsvater, C. E. & Carter, R. W. C. (1957), Discharge characteristics of rectangular thin plate weirs, J. Hydraulics Div. ASCE 83(HY6), 1453/1–1453/36.

Komar, P.D., 1987a. Selective grain entrainment by a current from a bed of mixed sizes: a reanalysis. J. Sediment. Petrol. 57, 203–211.

Kramer, H., Sand mixtures and sand movement in fluvial models, Trans. Am. Soc. Civ. Eng., 100, 798-878, 1935.

Lamb, M. P., W. E. Dietrich, and J. G. Venditti (2008), Is the critical Shields stress for incipient sediment motion dependent on channel-bed slope, J. Geophys. Res., 113, F02008, doi:10.1029/2007JF000831.

Miller, M.C., McCave, I.N., and Komar, P.D. (1977). "Threshold of sediment motion under unidirectional currents." Sedimentology, Vol. 24

Neill, C. R., and M. S. Yalin, Quantitative definition of beginning of bed movement, J. Hydraul. Div. Am. Soc. Civ. Eng., 95, 585-588, 1969.

Paphitis, D. (2001). "Sediment movement under unidirectional flows: an assessment of empirical threshold curves." Coastal Eng., Vol. 43

Parker, G., and P. C. Klingeman, On why gravel bed streams are paved, Water Resour Res.,1 8, 1409-1423, 1982

Recking, A. (2009), Theoretical development on the effects of changing flow hydraulics on incipient bed load motion, Water Resour. Res., 45, W04401, doi:10.1029/2008WR006826.

Shields, A.F. (1936). "Application of similarity principles and turbulence research to bed-load movement." Mitteilungen der Preussischen Versuchsanstalt für Wasserbau und Schiffbau, Berlin, Germany.

Stevens M.A., Simons, D.B. and Lewis, G.L. (1976) Safety Factors for Riprap Protection. J. of Hyd. Div., ASCE, 102(5), 637-655.

Sundborg, A., 1956. The river Klararven, a study of fluvial processes. Geogr. Ann. 38, 127–316.

Wathen, S. J., R. I. Ferguson, T. B. Hoey, and A. Werritty, Unequal mobility of gravel and sand in weakly bimodal river sediments Water Resour. Res., 31, 2087-2096, 1995

White, C. M., The equilibrium of grains on the bed of a stream, Proc. R. Soc. London A, 174, 322-338, 1940.

Whitehouse, R.J.S. and Hardisty, J. (1988) Experimental Assessment of Two Theories for the Effect of Bed slope on the Threshold of Bedload Transport. Marine Geology, vol. 79, 135-139.

Wiberg, P. L. & Smith, J. D. 1987 Calculations of the critical shear stress for motion of uniform and heterogeneous sediments. Water Resour. Res. 23 (8), 1471–1480.

Wilcock, P. R., Methods for estimating the critical shear stress of individual fractions in mixed-size sediment, Water Resour. Res., 24, 1127-1135, 1988.

Wilcock, P. R., Flow competence: A criticism of a classic concept, Earth Surf Processes Landforms,1 7, 289-298, 1992b.

Yalin, M.S. and Karahan, E. (1979). “Inception of sediment transport.”J. Hydraul. Div., Vol. 105, No. 11, pp. 1433-1443.